Ablation of oligodendrogenesis in adult mice alters brain microstructure and activity independently of behavioural deficits

Malte S. Kaller[1], Alberto Lazari[1], Yingshi Feng[1], Annette van der Toorn[2], Sebastian Rühling[1,3], Christopher W. Thomas[4], Takahiro Shimizu[5], David Bannerman[6], Vladyslav Vyazovskiy[4,7,8], William D. Richardson[5], Cassandra Sampaio-Baptista[1,9, #], Heidi Johansen-Berg[1, #]

1. Wellcome Centre for Integrative Neuroimaging, FMRIB, Nuffield Department of Clinical Neurosciences, University of Oxford, Oxford, United Kingdo; 2. Biomedical MR Imaging and Spectroscopy Group, Center for Image Sciences, University Medical Center Utrecht & Utrecht University, Utrecht, The Netherlands; 3. Department of Diagnostic and Interventional Neuroradiology, School of Medicine, Klinikum rechts der Isar, Technical University of Munich, Munich, Germany; 4. Department of Physiology, Anatomy and Genetics, University of Oxford, Oxford, United Kingdom; 5. University College London, The Wolfson Institute for Biomedical Research, London, United Kingdom; 6. Department of Experimental Psychology, University of Oxford, Oxford, UK; 7. Sir Jules Thorn Sleep and Circadian Neuroscience Institute, University of Oxford, Oxford, United Kingdom; 8. The Kavli Institute for Nanoscience Discovery, Oxford, United Kingdom; 9. School of Psychology and Neuroscience, University of Glasgow, Glasgow, United Kingdom.

 # Contributed equally

Abstract

Oligodendrocytes continue to differentiate from their precursor cells even in adulthood, a process that can be modulated by neuronal activity and experience. Yet, our understanding of the functional role of adult oligodendrogenesis remains limited. Previous work has indicated that conditional ablation of oligodendrogenesis in adult mice can lead to learning and memory deficits in a range of behavioural tasks. Our results, reported here, have replicated a key finding that learning to run on a complex wheel with unevenly spaced rungs is disrupted by ablation of oligodendrogenesis. However, using ex vivo MRI (MTR and DTI), we also found that ablating oligodendrogenesis by itself alters brain microstructure, independent of behavioural experience. Furthermore, in vivo EEG recording in behaviourally naïve mice with ablated oligodendrogenesis revealed altered brain activity in the form of increased EEG power density across a broad frequency range. Together, our data indicate that disrupting the formation of new oligodendrocytes directly alters brain microstructure and activity. This suggests a role for adult oligodendrogenesis in the maintenance of brain function and indicates that task-independent changes to brain structure and function might contribute to the learning and memory deficits associated with oligodendrogenesis ablation.

Introduction

Myelination of axons plays a critical role in the functioning of the vertebrate nervous system by increasing the transmission speed and energy efficiency of neural processing (Nave, 2010; Salzer and Zalc, 2016). Recent studies have demonstrated that myelin is more dynamic than initially thought. Myelination can be stimulated by artificially exciting neuronal activity (Cullen et al., 2021; Gibson et al., 2014; Mitew et al., 2018), indicating that myelin plasticity, in addition to synaptic modification, might be one way in which experience can shape brain structure and function (Bonetto et al., 2021; Kaller et al., 2017; Xin and Chan, 2020). Indeed, changes in myelination and white matter (WM) microstructure have been consistently associated with learning in humans (Lakhani et al., 2016; Scholz et al., 2009) and rodents (Bacmeister et al., 2022; Sampaio-Baptista et al., 2013). In addition, adaptive myelination is proposed to regulate homeostatic coordination and oscillatory self-organization in local and large-scale brain networks (Dubey et al., 2022; Noori et al., 2020; Pajevic et al., 2022, 2014; Talidou et al., 2022). Thus, deficient myelin plasticity might lead to alterations in myelination and neural network function that impair neurological function (Geraghty et al., 2019; Knowles et al., 2022). Yet, the questions of when, how, and to what extent adaptive myelination contributes to relevant changes in neural circuit function require further investigation.

Myelination can be adaptively modified through the formation of new oligodendrocytes (OLs), the myelin forming glial cells in the central nervous system (Bergles and Richardson, 2016; Foster et al., 2019). OLs continue to differentiate even in adulthood (Hill et al., 2018; Hughes et al., 2018; Rivers et al., 2008; Young et al., 2013) from populations of oligodendrocyte precursor cells (OPCs) that remain abundant, dynamic and widespread in the CNS throughout life (Dawson et al., 2003). Recently, multi-photon imaging studies in live behaving mice have demonstrated continuous formation of oligodendrocytes and changes in oligodendroglial cells dynamics in response to motor learning (Bacmeister et al., 2022; Hill et al., 2018; Hughes et al., 2018). However, the contribution of such continuous and adaptive oligodendrocyte lineage dynamics to the functioning of the nervous system is still not well understood.

Transgenic mouse lines that allow conditional ablation of oligodendrogenesis in early adulthood have provided information about the causal involvement of new oligodendrocyte formation in behaviour. The first use of this transgenic approach revealed that mice with ablated oligodendrogenesis have an impaired ability to learn to run at speed on a complex wheel, suggesting a deficit in motor skills learning (McKenzie et al., 2014; Xiao et al., 2016). Subsequent studies found that interrupting OL generation also leads to deficits in long-term consolidation of spatial and fearful memories (Pan et al., 2020; Steadman et al., 2020). Additionally, reduced opioid reward learning (Yalçın et al., 2022) and impaired training-induced improvements in spatial working memory have also been reported (Shimizu et al., 2023). However, if and how the disruption of oligodendrogenesis in adulthood affects the CNS, independent of experience in a specific task, remains understudied.

65 The current study set out to further probe our understanding of behavioural, anatomical and physiological
66 consequences of disrupting the formation of new OLs during adulthood. Our first aim was to replicate key
67 findings indicating a motor learning deficit in adult mice with ablated oligodendrogenesis on the complex
68 wheel task (McKenzie et al., 2014; Xiao et al., 2016). Our results replicated the finding that ability to perform
69 a complex wheel (CW) running task is perturbed within the first hours of testing in animals with disrupted
70 oligodendrocyte. Our second aim was to study how genetic ablation of OL differentiation affects brain
71 microstructure and activity in adult mice using *ex vivo* magnetic resonance imaging (MRI) and *in vivo* EEG
72 recording. We hypothesised that disruption of new oligodendrocyte formation alters the metrics of brain
73 microstructure sensitive to myelin and, as a consequence, might modify cortical network activity. We
74 investigated how learning to run the complex wheel affects brain microstructure in the presence and
75 absence of ongoing OL differentiation, probing the mechanism by which adaptive OL formation might
76 contribute to skill acquisition. We found alterations in both the microstructure and activity of the brain in
77 animals with disruptioned oligodendrogenesis, irrespective of animal's experience with the CW task.

78 **Results**

79 ***Deleting Myrf in OPCs leads to ablation of oligodendrogenesis***

80 In the current study, we used a transgenic mouse model that allowed conditional deletion of myelin
81 regulatory factor (*Myrf*) in the resident PDGFRα-positive OPC population (*Pdgfra-CreER*^{T2}*:R26R-YFP: Myrf*$^{(fl/fl)}$;
82 referred to as 'P-Myrf' from here on; McKenzie et al., 2014). As *Myrf* encodes a transcription factor required
83 for oligodendrocyte differentiation (Emery et al., 2009), animals with both alleles of *Myrf* conditionally
84 deleted during adulthood (P-Myrf$^{(-/-)}$) have markedly reduced formation of new oligodendrocytes 6 weeks
85 after tamoxifen treatment, as compared to control animals with one functional allele (P-Myrf$^{(+/-)}$) (Fig. 1A-D).

86 ***Ablation of oligodendrogenesis leads to impaired performance on the complex wheel***
87 Previous work has indicated that such conditional ablation of oligodendrogenesis in adult mice leads to
88 learning deficits in a range of different behavioural tasks (McKenzie et al., 2014; Pan et al., 2020; Steadman
89 et al., 2020). We aimed to re-examine the ability of such mice to learn to run on a complex running wheel
90 with irregularly spaced rungs (McKenzie et al., 2014; Xiao et al., 2016) (Illustrated in Fig. 2A).

91 A total of 124 animals (P-*Myrf*$^{(+/-)}$; n=59, 28 females; P-*Myrf*$^{(-/-)}$; n=65, 29 females) were tested on the
92 complex wheel (CW) across several experiments (see Methods). Animals received tamoxifen in early
93 adulthood (age range: P60-90) and behavioural performance was tested 3-6 weeks later (Fig. 2C).

94 To investigate whether ablation of *Myrf* in OPCs during adulthood impacts performance on the complex
95 running wheel, we tested for main effects of genotype, time and interactions on daily average and maximum
96 speed using a mixed-two way ANOVAs. Sex was included as an additional between-subject factor.

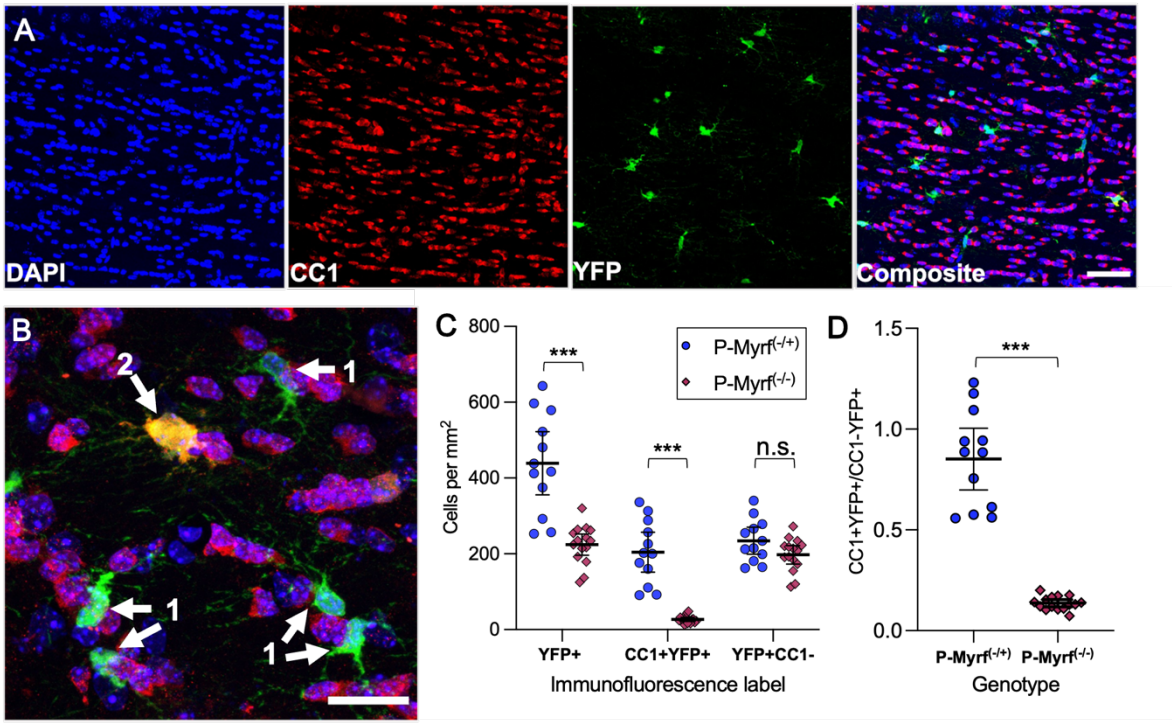

Fig. 1. **Deleting Myrf in OPCs significantly reduced the formation of new oligodendrocytes. (A)** Representative individual image of immunohistochemistry, split into its separate channels. DAPI was used to identify individual cell nuclei, CC1 was used to label mature oligodendrocytes, and YFP marked OPCs at the time of tamoxifen administration (Scale bar 50 um). **(B)** CC1+ and YFP+ cells were quantified and labelled as either (1) an OPC that remained YFP+|CC1-, or (2) a recently matured Oligodendrocyte that was YFP+|CC1+. **(C)** Quantification confirmed a significant reduction of the density of YFP+|CC1+ recently matured oligodendrocytes in the P-Myrf$^{(-/-)}$ animals 6 weeks after tamoxifen administration. **(D)** The ratio between recently matured Oligodendrocytes (YFP+|CC1+) and labelled OPCs (YFP+|CC1-) was significantly lower in the P-Myrf$^{(-/-)}$. Data presented as Mean±95%CI, Welch's two sample t-test used for statistical comparison. *** represents statistical significance of p<0.001. P-Myrf$^{(+/-)}$, n=12; P-Myrf$^{(-/-)}$, n=15.

Supplementary Table 2 contains comprehensive information on the statistical analysis methods utilized and the corresponding results for each dataset.

A main effect of genotype for average speed (F(1,120)= 10.00, *p*=0.002, Fig. 2D) and maximum speed ((F(1,120)=11.92, p<0.001, Fig. 2E) over 8 days confirmed that overall performance metrics of P-*Myrf*$^{(-/-)}$ animals were lower than for their P-*Myrf*$^{(+/-)}$ siblings. Furthermore, P-*Myrf*$^{(-/-)}$ animals had impaired capacity to improve their performance with practice over training days (mixed two-way ANOVA, time*genotype interaction for average daily speed (F(2.74,328.5)=5.56, *p*=0.001, Fig. 2D) and maximum daily speed F(2.57,308.9)=4.76, *p*=0.005, Fig. 2E). Females outperformed males in terms of running performance (main effect of sex, average speed: F(1,120)= 13.1, p<0.001, maximum speed: F(1,120)= 17.5, p<0.001, Suppl. Fig. 1G) and spent more time on the complex running wheel (Suppl. Fig. 1H, Mann-Whitney U, *p*=0.014), yet no statistically significant interaction between animals' sex and genotype was detected in any ANOVA test presented. Running ability on a normal running wheel and general motor skills, as tested by RotaRod and

Balance Beam, were not impaired in the P-Myrf$^{(-/-)}$ animals (Suppl. Fig. 1A-F), indicating that performance differences between genotypes did not generalize to other running tasks or tests of motor skill.

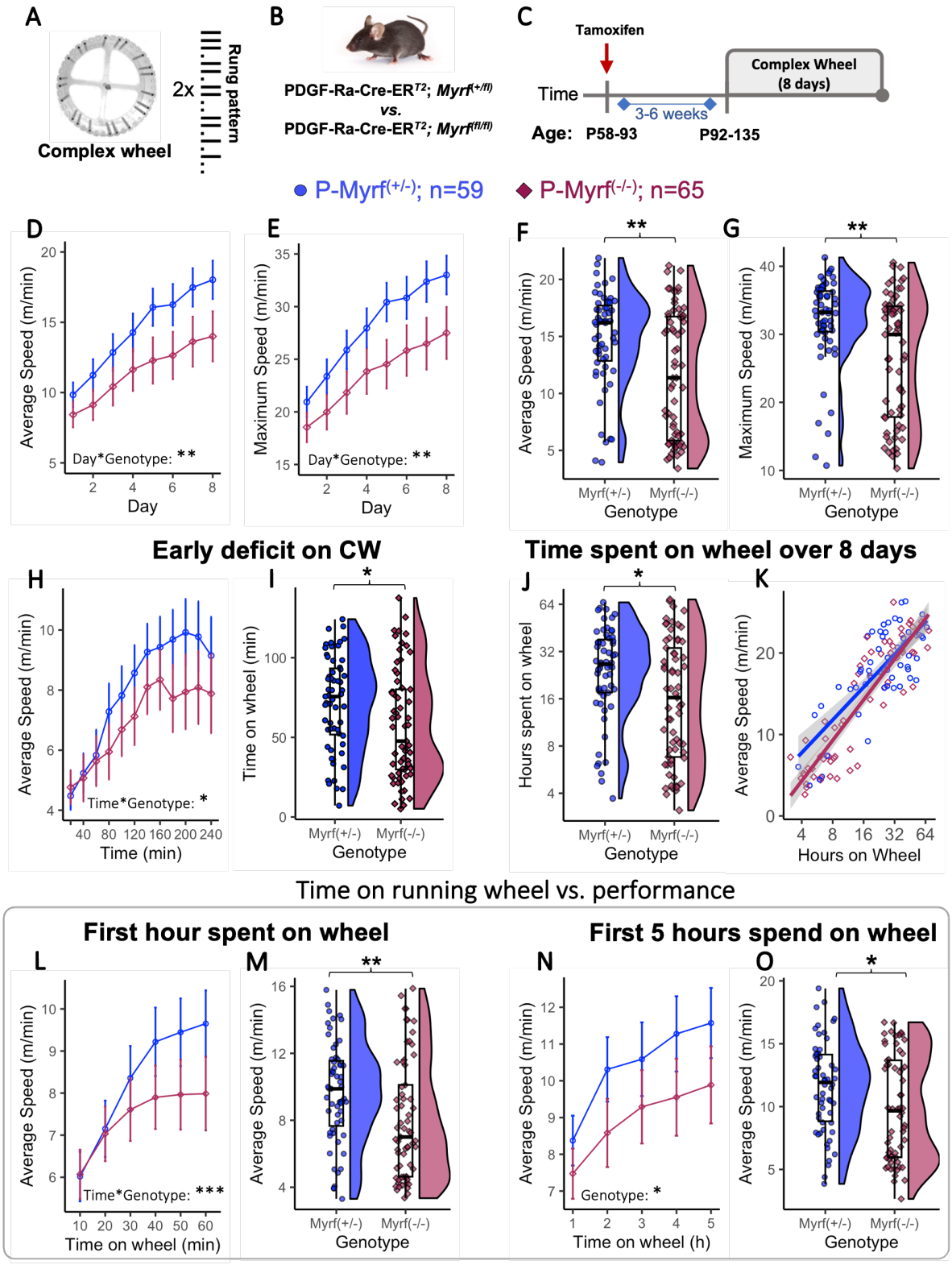

Fig. 2. ***Preventing differentiation of new OL leads to impaired performance on the complex wheel. (A)*** *Complex running wheel, with an irregular rung pattern displayed beside the wheel.* ***(B)*** *Animals bred on a PDGF-Rα-Cre-ER^{T2} back-*

ground with two floxed alleles of Myrf were compared to control animals that only have a single allele floxed. ***(C)*** *Schematic Illustration of experimental design**.** Between 3-6 weeks after tamoxifen treatment, animals were given free access to the CW for 8 days.* ***(D)*** *Mean average speed and* ***(E)*** *maximum speed on the complex wheel of P-Myrf$^{(-/-)}$ was lower across 8 days. A statistically significant effect of Genotype and for Genotype*time interaction was detected for both speed metrics.* ***(F, G)*** *Raincloud plots of Average* ***(F)*** *and Maximum* ***(G)*** *speed across the 8 days of running.* ***(H)*** *Average running speed on the CW during the first 4 hours. P-Myrf$^{(-/-)}$ had a significantly lower speed improvement over the first 4 hours (Time*Genotype interaction).* ***(I)*** *Time spent on the wheel within the first 4 hours showed large variability and was lower within the P-Myrf$^{(-/-)}$ group (Mann-Whitney U, p=0.013).* ***(J)*** *P-Myrf$^{(-/-)}$ spent less time running on the complex wheel than their P-Myrf$^{(+/-)}$ siblings over 8 days of testing.* ***(K)*** *Statistically significant log relationship between the average speed of animals on day 8 of testing and the time animals spend on the wheel during the 8 days.* ***(L)*** *Average running speed plotted against the first hour of time animals spent on the wheel.* ***(M)*** *Average speed within 10 mins time period of wheel running after the first hour on the wheel.* ***(N)*** *Average running speed plotted against the time animals spend on the wheel for the first 5 hours (P-Myrf$^{(+/-)}$; n=58 ; P-Myrf$^{(-/-)}$; n=64).* ***(O)*** *Average speed within 1 hour of wheel running after 5 hours on the wheel. Data presented as Mean±95%CI or boxplots. Mixed-ANOVA (Main Factors: Genotype, Sex; Factor: Time) used for statistical comparison of performance over time comparison. Mann-Whitney U test used for statistical comparison of two groups. Asterix indicate statistical significance (*p<0.05, **p<0.01, ***p<0.001).*

The average running speed (Fig. 2F) and maximum running speed (Fig. 2G) across the 8 days of training was lower in P-*Myrf*$^{(-/-)}$ (Mann-Whitney U: average speed, Fig. 2F, p=0.003; maximum speed, Fig. 2G, p=0.002), further indicating a deficit in performance on the CW in animals with ablation of *Myrf* in OPCs during adulthood. However, the distribution of performance values was not equal between genotype groups, with higher variability and a bimodally shaped distribution especially prominent in the group of P-*Myrf*$^{(-/-)}$ animals (Fig. 2F & G), a feature that was also reported by McKenzie et al. (2014).

Furthermore, the observed deficit on the CW was already detectable within the first 4 hours of exposure to the wheel (Mixed ANOVA: Genotype*Time F(4.83, 579.6) = 2.63, p=0.025, Fig. 2H), replicating an early deficit in complex wheel learning previously reported by Xiao et al (2016).

P-Myrf$^{(-/-)}$ animals spend less time running on the complex wheel

As running on the wheel was voluntary and animals were given unrestricted access to the wheels, the time individual animals spent on the running wheel varied significantly. Indeed, within the first 4 hours of exposure to the wheel, the time animals spent rotating the wheel ranged from about 5 minutes to over 2 hours (Fig. 2I). Interestingly, P-*Myrf*$^{(-/-)}$ animals spent significantly less time on the wheel within this 4 hour period (Fig. 2I, Mann-Whitney U, p=0.013). A similar trend was observed over the 8 days of testing. Time running on the wheel ranged from around 4 hours to about 64 hours (Fig. 2H) and P-*Myrf*$^{(-/-)}$ animals spent less time running on the complex running wheel than P-*Myrf*$^{(-/+)}$ (Mann-Whitney U: p=0.014, Fig. 2H, also see Suppl. Fig. 1I). Similar to other performance metrics across 8 days (Fig. 2F & G), the time animals spent on the wheel had a wider and bimodal distribution in the P-*Myrf*$^{(-/-)}$ group (Fig. 2H).

Importantly, we found a statistically significant log-positive relationship between the time animals spent running on the wheel and their average running speed on day 8 of testing (Fig. 2I, Spearman's rank correlation, across genotype, rho = 0.800, p<0.001; P-*Myrf*$^{(+/-)}$, rho=0.627, p<0.001; P-*Myrf*$^{(-/-)}$, rho=0.871 p<0.001). This suggests that when considering running speed metrics over chronological time periods (e.g.

153 days, Fig. 2D & E) it might be important to account for variation in the time animals spent running on the
154 wheel, and therefore inter-individual variation in the time available for learning the task.

155 ***Deficit on complex running wheel detected within the first hours of running***

156 One way to account for such variation is to compare running performance of animals against the time they
157 spent on the wheel, rather than chronological time. Hence, we analysed average running speed on the
158 complex wheel for the first hour animals spent running on the wheel, regardless of when that running
159 happened (Fig. 2 L & M). Using a mixed two-way ANOVA (main factors: genotype, sex; within subject factor:
160 time(10 min intervals)), we found a significant effect of time ($F(2.21, 265.3)= 88.0$, $p<0.001$) and a significant
161 time*genotype interaction for average daily speed ($F(2.21, 265.3)= 9.06$, $p<0.001$, Fig. 2J), indicating that P-
162 *Myrf*$^{(-/-)}$ animals showed less improvement in performance with practice over the first hour of running. The
163 average running speed achieved in a 10-minute interval after 1 hour on the wheel was significantly lower in
164 P-*Myrf*$^{(-/-)}$ animals (Fig. 2K, Mann-Whitney U: $p= 0.004$).

165 As this deficit is prominent within the first hour spent running on the complex wheel, we wondered how the
166 genotype differences changed over subsequent time animals spent on the wheel. Comparing performance
167 across the first 5 hours running on the wheel, P-*Myrf*$^{(-/-)}$ animals had a persistent lower average running
168 speed than P-*Myrf*$^{(+/-)}$ controls (Fig 2 L-O). A mixed two-way ANOVA (main factors: genotype, sex; within
169 subject factor: time) confirms a statistically significant effect of time (average speed: $F(2.2,259.9)= 53.8$,
170 $p<0.001$) and for genotype (average speed: $F(1,118)= 4.99$, $p=0.027$, Fig. 2N), yet not for an interaction
171 between time spent on the wheel and the animals' genotype that might indicate a deficit in learning ability
172 over this time period (average speed: $F(2.2,259.3)= 1.22$, $p=0.29$). The running speeds in the 5th hour of
173 running on the wheel was different between genotypes (average speed: Mann-Whitney U: $p= 0.031$, Fig.
174 2O). This suggests the group differences that became apparent within the first hour on the wheel (Fig.
175 2L&M) persisted over subsequent hours of running.

176 Overall, these results replicate the main behavioural results obtained by McKenzie et al (2014) and Xiao et al
177 (2016), indicating an early deficit in learning on the CW in animals with ablation of *Myrf* in OPCs during
178 adulthood. However, unlike McKenzie et al. (2014), we found wide variation in the amount of time animals
179 spent engaging with the task, a factor that is important to take into account when interpreting behavioural
180 changes. Taking this variation into account by considering time spent on wheel rather than chronological
181 time, we found that ablation of oligodendrogenesis results in deficits in performance improvement over the

182 first hour of experience on the wheel. These deficits are maintained, but not exacerbated, over subsequent
183 hours of experience.

184 **Probing task demands of the complex wheel task**

185 To better understand the task demands of the wheel running task, we tested wild type (WT) mice on
186 different variants of the wheel. Switching to a complex wheel after running on the normal wheel leads to a
187 partial reduction in running speed in WT mice (Suppl. Fig. 5), that recovers after a day or two of further
188 training, indicating the task demand specific to the CW is mainly probed in the first couple of days of
189 exposure to the wheel.

190 To test whether mice learn a specific sequence of movements to master the complex wheel, we tested the
191 effects of changing the rung sequence after exposure to one variant of the complex wheel. This does not
192 lead to reduction in running speed in WT mice (Suppl. Fig. 6), suggesting that mice learn a general strategy
193 for running on irregularly spaced rungs, rather than a specific sequence of movements.

194 Taken together, these behavioural findings in WT mice suggest that learning to run at speed on a complex
195 wheel primarily involves adaptation to the irregular spaced rung positions, particularly in the early days of
196 testing.

197 ***Ablation of oligodendrogenesis alters brain microstructure independently of wheel running***

198 Previous work has reported alterations in white matter microstructure, measured with MRI techniques, in
199 response to motor learning (Sampaio-Baptista et al., 2020, 2013). However, the underlying mechanism is
200 unclear, as these changes could relate to remodelling of pre-existing myelin and/or recruitment of new
201 oligodendrocytes. Furthermore, the contribution of new oligodendrocytes to MRI metrics has not been
202 directly tested.

203 In the current study we hypothesised that disruption of oligodendrogenesis in early adulthood affects brain
204 microstructure, as it interferes with ongoing cellular dynamics and *de novo* myelination. Further, we
205 hypothesised that learning to run on the CW affects brain microstructure. Finally, given evidence that
206 adaptive oligodendrogenesis contributes to learning to run on the CW, we hypothesised that effects of CW
207 running on brain microstructure should differ between knock-outs and controls.

208 We employed *ex vivo* MRI (see Methods) to compare P-Myrf$^{(-/-)}$ (n=26) and P-Myrf$^{(-/+)}$ (n=25) animals that
209 had free access for 12 days to either the complex wheel (CW, n=26) or to a fixed immovable CW in which
210 running was not possible (from here on referred to as 'fixed wheel', FW, n=25, Fig. 3A). This FW control

condition was used to keep all environmental factors, other than wheel running, similar between groups (schematic illustration of experimental design, Fig. 3B).

Brain microstructure was assessed *ex vivo* using a 9.4 T horizontal bore MR scanner (Varian, Palo Alto, CA, USA). Magnetisation transfer imaging and diffusion-weighted imaging were acquired. Three parameters were extracted (see Suppl. Fig. 2): i) magnetisation transfer ratio (MTR), which allows indirect detection of water bound to macromolecules, such as lipids and proteins, and is thus sensitive to myelin (Deloire-Grassin et al. 2000); ii) fractional anisotropy (FA), which describes the anisotropy of diffusion of water molecules; and iii) mean diffusivity (MD), which describes the rotationally invariant magnitude of water diffusion within brain tissue. FA and MD are sensitive but

not specific to a number of white matter features, such as myelin, axon calibre, density and organisation, among others (Lazari and Lipp, 2021; Sampaio-Baptista and Johansen-Berg, 2017; Zatorre et al., 2012).

For a region of interest (ROI) analysis, five brain areas hypothesised to be involved in learning a running wheel task, or sensitive to exercise on the wheel, were selected: primary (M1) and secondary (M2) motor cortex, primary sensory cortex (S1), hippocampus (Hipp) and an anterior region of the corpus callosum (antCC), as illustrated in Fig. 3C. For exploratory purposes, we ran voxel-wise analyses to test for more local effects in any brain area across the grey matter mask and white matter skeleton (Fig. 3F). Finally, to investigate global changes, we tested for effects averaged across the whole grey matter (GM) and whole white matter (WM) skeleton (Fig. 3G,H).

Effects of genotype: First, to investigate the effect of the genetic manipulation on brain microstructure without considering behavioural experience of wheel running, we tested for effects of genotype in animals that were only exposed to the fixed wheel (FW, our control condition, n=25). When testing across the four grey matter regions of interest (ROIs) (M1, M2, S1, Hipp), P-Myrf$^{(-/-)}$(n=13) were found to have significantly lower MTR, compared to P-Myrf$^{(+/-)}$ (n=12) (mixed ANOVA; main effect of genotype ($F(1,17)=7.32$, $p=0.015$). Post hoc tests for individual ROIs (ANOVA, Bonferroni adjusted for number of ROIs) found a significant reduction in MTR in M1 (Fig. 3D, $p=0.02$) and M2 (Fig. 3D, $p=0.032$). Additionally, for the white matter region of the anterior corpus callosum (antCC), P-Myrf$^{(-/-)}$ had significantly lower MTR, compared to P-Myrf$^{(+/-)}$ (Fig. 3E, $p=0.013$). No statistically significant changes between groups were observed for diffusion-derived metrics of MD and FA (Suppl. Fig. 3). No effects were found in the voxel-wise analysis.

Effects of wheel condition: Next, to investigate the effect that running the complex wheel for 12 days may have on brain microstructure, we tested for effects of wheel condition (fixed vs complex wheel) in P-Myrf$^{(+/-)}$ control animals only (CW:n=13, FW: n=12). No statistically significant difference between the two running wheel groups were detected in MTR, FA or MD in the ROI analysis (Suppl. Fig 3). A voxel-wise analysis

243 revealed an increase in MD in the left M1 grey matter region (Suppl. Fig. 4A & B) for P-Myrf$^{(+/-)}$ that ran the

244 complex wheel.

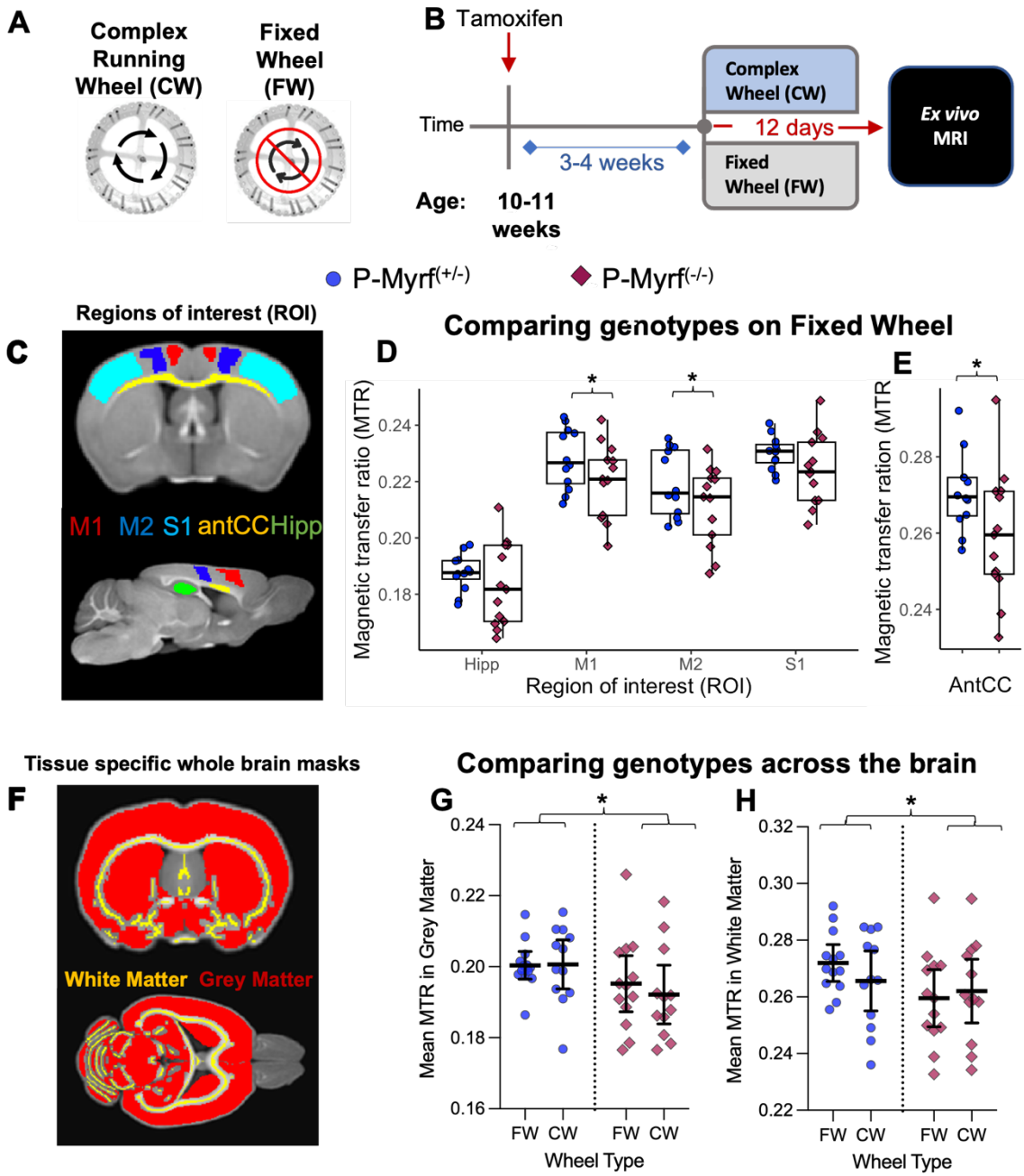

Fig. 3. ***Ablation of oligodendrogenesis alters brain microstructure even in the absence of wheel running. (A)*** *Animals used for ex vivo MRI imaging were exposed to either a complex wheel on which they can run, or an immovable complex wheel (Fixed Wheel, FW).* ***(B)*** *Illustration of experimental design.* ***(C)*** *Coronal and sagittal section of MTR image illustrating Regions of Interest (ROI) masks used for the ROI analysis.* ***(D)*** *For animals only exposed to the Fixed Wheel (FW, P-Myrf$^{(+/-)}$, n=12, , P-Myrf$^{(-/-)}$, n=13) , ROI-specific mean MTR revealed that the ablation of oligodenrogenesis in the absence of wheel running lead to statistically significant changes in brain microstructure in the Primary motor cortex (M1), Secondary motor cortex (M2) and the* ***(E)*** *anterior corpus callosum (antCC).* ***(F)*** *Mask for the Grey Matter (GM, red) and White Matter skeleton (WM, yellow) used for analysis.* ***(G-H)*** *MTR was reduced in* ***(G)*** *GM and the* ***(H)*** *WM skeleton for P-Myrf$^{(-/-)}$ animals compared to control animals, regardless of wheel condition (FW, P-Myrf$^{(+/-)}$, n=25, , P-Myrf$^{(-/-)}$, n=25). Diffusion-weighted parameters, such as FA and MD, did not reveal any statistically significant differences. See Suppl. Fig. 3 for more details. Data presented as Mean±95%CI or boxplots. M1:Primary Motor Cortex, M2:Secondary Motor Cortex, S1: Primary Somatosensory Cortex, antCC: Anterior Corpus Callosum. Asterix indicate statistical significance (*p<0.05).*

245 *Interactions between genotype and wheel condition:* Finally, to investigate potential interactions between
246 genetic manipulation and behavioural experience, we performed an ANOVA with genotype and wheel (CW &
247 FW) as factors on all samples. Similar to effects found when considering the FW groups alone, significant
248 main effects of genotype on MTR were found within specific grey matter and white matter ROIs (M1, M2, S1,
249 antCC; Supp. Fig. 3A-E), as well as across the whole grey matter mask (Fig. 3G; F(1, 34)=7.77, *p*=0.019) and
250 the white matter skeleton (Fig. 3H; F(1,34)=4.73, 0.037). , with P-Myrf$^{(-/-)}$ animals having significantly lower
251 MTR. However, no main effect of wheel or interactions between genotype and wheel on MTR were found.
252 No main effects or interactions were detected in FA or MD in the ROI analysis (Suppl. Fig. 3F-N). The voxel
253 wise analysis detected small clusters of changes in MTR between genotypes in cortical and midbrain regions
254 (Suppl. Fig. 4C), yet no interaction between genotype and wheel was found for any voxel-wise analyses.

255 *Correlations between MRI and behavioural performance:* A voxel-wise analysis across all animals in the CW
256 condition (n=26) tested for correlations between brain metrics and performance metrics (maximum speed &
257 total distance run over 8 days). No relationship was found for MTR or FA. We found a negative correlation
258 between distance run and MD in broad areas in cortical grey matter and basal ganglia, independent of
259 genotype (Suppl. Fig. 3D&E). Mice that ran longer distances had lower MD, indicating that water in these
260 areas is more restricted (regardless of direction), potentially indicating higher brain tissue density.

261 Taken together, these results indicate that the ablation of oligodendrogenesis in young adult mice for 5-6
262 weeks led to decreases in the myelin sensitive metric MTR, across grey matter and white matter regions.
263 However, we found no interactions between wheel running and genotype, suggesting no evidence for
264 changes in brain microstructure in response to wheel running that depend on oligodendrogenesis.

265 ***Ablation of oligodendrogenesis changes oscillatory brain activity in Myrf-cKO mice in vivo***

266 Previous work has indicated that even subtle deficits in myelination can lead to altered neuronal activity and
267 synchronicity (Dubey et al., 2022; Gould et al., 2018; Kato et al., 2020), while modelling approaches indicate
268 a role of activity-dependent myelination in oscillatory self-organization and homeostatic coordination of
269 brain networks (Noori et al., 2020; Talidou et al., 2022).

270 As our histological and MRI data suggests altered myelination in P-Myrf$^{(-/-)}$ mice, we tested oscillatory brain
271 activity using cortical EEG recordings in freely-behaving P-Myrf mice, not exposed to running wheels. In each
272 animal, the electrodes were implanted in two cortical regions (see Fig. 4A) at the age of P110-120, 5-6 weeks
273 after tamoxifen treatment (Fig. 4B). Mice were individually housed in standard conditions. Data were

recorded over a 2-day period, 1-2 weeks after surgery (P-Myrf$^{(+/-)}$: n=3, P-Myrf$^{(-/-)}$: n=4) during spontaneous sleep and waking in undisturbed animals.

Spectral analysis revealed a significant increase in EEG spectral power across broad frequency bands in P-Myrf$^{(-/-)}$ animals in the frontal and occipital region during wakefulness (Fig. 4C-E), when compared to P-Myrf$^{(+/-)}$ animals. Using a Mixed ANOVA (Main effect: genotype, within-subject factor: electrode location), the genotype difference in total EEG power density in 1-30 Hz frequency range was statistically significant across both cortical derivations during wakefulness (main effect for genotype: $F(1,5)=10.4$, $p=0.023$). This change in total spectral power induced by the conditional deletion of *Myrf in OPCs* was also observed during other vigilance states such as REM sleep (Fig. 4F, Suppl. FigA&B; $F(1,5)=12.7$, $p=0.016$) and nonREM sleep (Fig. 4G, Suppl. Fig. C&D,$F(1,5)=11.4$, $p=0.02$). The fraction of time animals spent in different vigilance states did not differ between genotypes (Fig. 4H). The peak EEG power density during wake and REM sleep (0.25 hz resolution) in the Theta range (4-12 hz) was significantly different between genotype groups ($F(1,5)=7.4$, $p=0.041$, Suppl. Fig. 5E), yet the frequency of the peak was not (Suppl. Fig 5F). Altogether, these results provide evidence for changes in brain electrophysiology induced by the ablation of oligodendrogenesis for 7-8 weeks prior to EEG recording in freely moving and behaviourally naïve mice.

In summary, we replicated the previously reported behavioural phenotype of P-Myrf$^{(-/-)}$ showing reduced capacity to improve performance over time on the complex wheel, which is prominent within the first hours of running. We additionally found a high degree of variation in engagement with the wheel, which should be taken into account when interpreting results. Further, our results suggest that ablation of oligodendrogenesis alters brain microstructure, as detected by a reduction in MTR, and brain activity, as indicated by increase in EEG mean spectral power, independently of behavioural experience on the complex running wheel. This suggests ablation of oligodendrogenesis in P-Myrf$^{(-/-)}$ can itself lead to physiological and structural alterations in the brain.

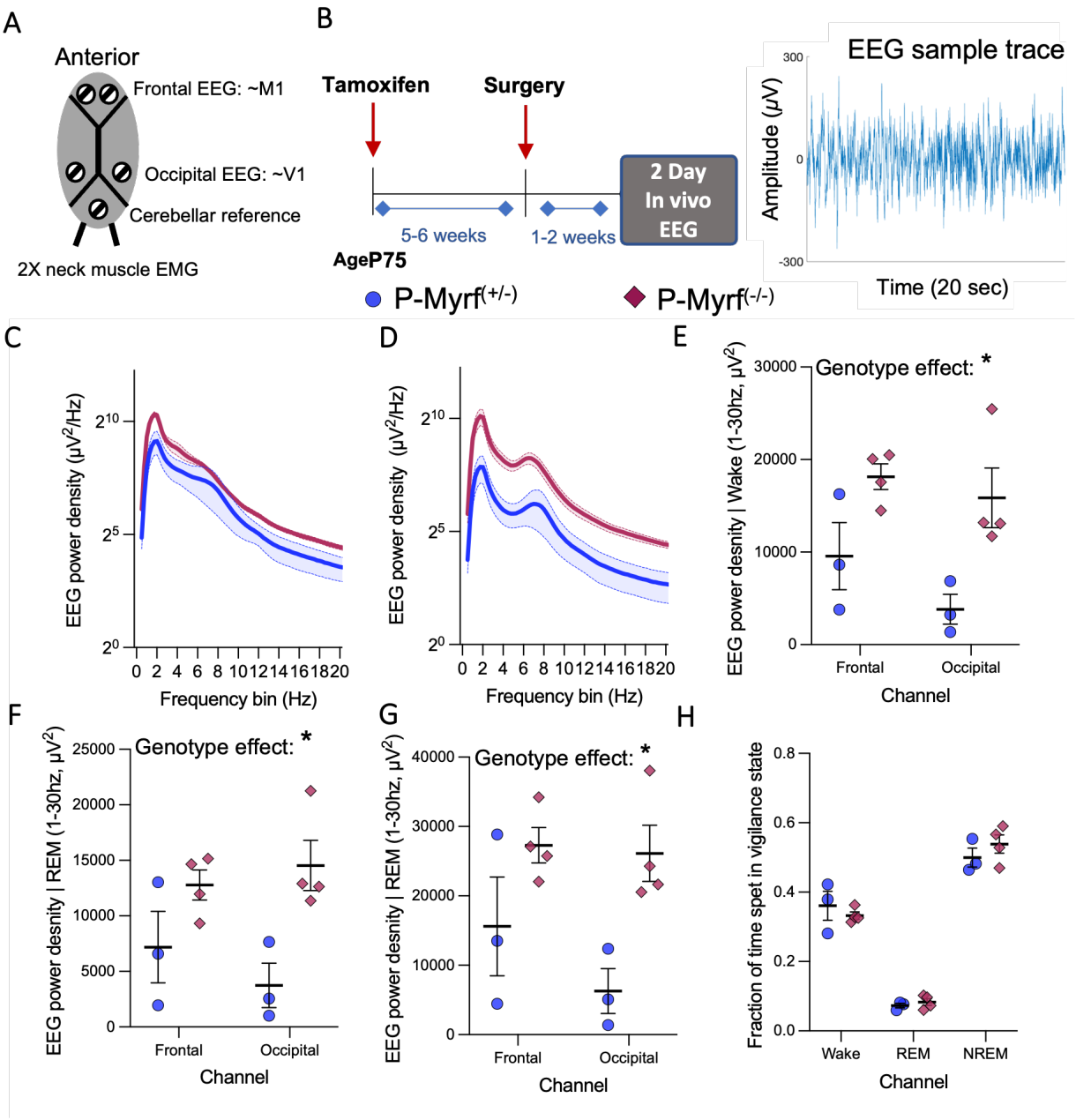

Fig. 4. ***Ablation of oligodendrogenesis alters brain activity in the absence wheel running. (A)*** *Schematic illustration of the location of screws implanted for in vivo EEG recording.* ***(B)*** *Schematic illustration of experimental design.* ***(C-D)*** *Mean group Power Spectral Density (PSD) by Frequency during wakefulness in* ***(C)*** *frontal channel and* ***(D)*** *occipital channels. Data presented as Mean±SED (**E**) The mean PSD across the 1-30 hz frequency bands was lower for animals with ablated oligodendrogenesis in the frontal and occipital channel during wakefulness. This genotype difference was found to be statistically significant across frontal and occipital channels (Mixed ANOVA) during wakefulness.* ***(F-G)*** *The effect was not specific to wakefulness, as statistically significant differences in mean PSD were also observed during* ***(F)*** *REM sleep and* ***(G)*** *non-REM sleep.* ***(H)*** *The fraction of time animals spent in different vigilance states. Recordings were undertaken in seven male adult mice (P-Myrf$^{(-/-)}$: n=4; P-Myrf$^{(+/-)}$: n=3). Data presented as Mean±SD. Asterix indicate statistical significance (*p<0.05).*

303 **Discussion**

304 This study investigated the consequences of disrupting OL differentiation during adulthood (Fig. 1) on
305 behaviour (Fig. 2), brain structure (Fig. 3) and brain activity (Fig. 4). Our results replicated the key finding that
306 ability to perform a complex wheel (CW) running task is disrupted by ablation of oligodendrogenesis (Fig. 2,
307 McKenzie et al., 2014; Xiao et al., 2016). These group differences on the complex wheel were present within
308 hours of running on the wheel. Additionally, using *ex vivo* MRI (Fig. 3) and *in vivo* EEG (Fig. 4), we found that
309 the ablation of oligodendrogenesis altered brain microstructure and activity independently of the
310 behavioural experience of running the complex wheel. Taken together, our findings indicate that inhibiting
311 the formation of new oligodendrocytes in adult mice not only led to a decline in performance on the
312 complex wheel but also brought about alterations in both the microstructure and activity of the brain,
313 irrespective of animals' experience with the task. Whether and how these task-independent changes in brain
314 microstructure and function contributed to the observed behavioural phenotype requires further
315 investigation.

316 ***Replication of behavioural deficit on the complex wheel***

317 We found large variability in the time animals spent engaging with the complex wheel task, which was in
318 turn related to their overall performance (Fig. 2I). Accounting for this variability by analysing performance on
319 the CW as a function of time animals spent on the CW (Fig. 2L-O) revealed that P-Myrf$^{(-/-)}$ animal's deficit on
320 the wheel arises within the first hour of running (Fig. 2L-<).

321 However, it is difficult to clearly define the underlying deficit in P-Myrf$^{(-/-)}$ mice that leads to the observed
322 deficit on the CW, as the task demands of the CW are multifaceted. . Running speed improvements over
323 several days are observed on both the normal and complex wheel and can therefore reflect generic aspects
324 of wheel exposure as well as specific demands of the complex wheel (Suppl. Fig 1D, Suppl. Fig. 6). Switching
325 from a normal wheel to a complex wheel leads to a temporary reduction in running performance in WT mice
326 (Suppl. Fig. 6, Hibbits et al., 2009), indicating there is some specific task demand of the irregular spaced
327 rungs. Yet, changing the rung sequence does not affect performance, indicating that mice adapt a strategy
328 to cope with irregular spaced rungs in general and do not learn a specific sequence (Suppl. Fig 6). Together,
329 this indicates that mice need to find a new strategy (e.g. adapt their gait pattern, McKenzie et al., 2014) to
330 cope with irregular rungs and be able to run and improve their performance on the CW.

331 A deficit within the first hour running the complex wheel suggests that a key task requirement impaired in P-
332 Myrf$^{(-/-)}$ animals is probed by early attempts to perform the CW task, rather than by learning processes
333 evolving over several hours or days. Although the CW has been used as a test of subtle deficits in complex
334 motor *execution* (Hibbits et al., 2009; Liebetanz et al., 2007; Schalomon and Wahlsten, 2002), the fact that
335 P-Myrf$^{(-/-)}$ mice already trained on the CW prior to tamoxifen treatment have no deficits when re-exposed to

336 the CW (McKenzie et a l., 2014), together with the absence of any execution deficit on other motor tasks
337 (Suppl. Fig. 1A-F, McKenzie et al., 2014), suggests that impairment that we and others have found in CW
338 performance reflects impairment in the acquisition of a new skill rather than skill execution or general
339 motor performance.

340 ***Task-independent changes to brain structure and function might contribute behavioural deficit***

341 How an inability to form new oligodendrocytes can cause the observed learning phenotype of P-Myrf$^{(-/-)}$ mice
342 within just a few hours is unclear. Previous studies suggest that rapid production of *Enpp6*-expressing
343 immature oligodendrocytes can be observed within the first hours of exposure to the complex wheel,
344 potentially contributing to circuit functioning and neuronal metabolism (Xiao et al., 2016). Yet, our
345 understanding of how new oligodendrocytes contribute to skill learning and memory formation remains
346 incomplete, with apparently different timescales of involvement found with different learning paradigms.
347 For example, while early learning deficits have been found with complex wheel running, studies investigating
348 spatial learning and fear conditioning in mice with a conditional knockout of *Myrf* in OPCs found no deficit in
349 early memory formation, but a deficit of memory consolidation over days or weeks (Pan et al., 2020;
350 Steadman et al., 2020). Different aspects of myelin plasticity might occur over distinct timescales. For
351 example, a study investigating motor learning in the dextrous reaching task found modulation of existing
352 myelin in upper layers of M1 predominant in early stages of learning, while addition of new myelin sheaths
353 was more relevant post learning (Bacmeister et al., 2022).

354 An alternative explanation for the behavioural deficit is that the disruption of oligodendrogenesis for weeks
355 prior to behaviour testing in P-Myrf$^{(-/-)}$ caused subtle changes in brain microstructure (Fig. 3) and activity (Fig.
356 4) which then impacted on capacity to learn a new skill. New oligodendrocytes (OLs) continue to
357 differentiate throughout early adulthood (Hill et al., 2018; Hughes et al., 2018; Rivers et al., 2008; Young et
358 al., 2013) and interfering with such ongoing cellular dynamics can have unintended consequences, as
359 suggested by the current study (Fig. 3 & Fig. 4). Activity-regulated myelination, including oligodendrogenesis,
360 is proposed to play a role in homeostatic coordination and oscillatory self-organization in local and large-
361 scale brain networks (Dubey et al., 2022; Noori et al., 2020; Talidou et al., 2022) and mild impairments in
362 myelination have been linked to decreased motor learning by increasing asynchrony and spontaneity in
363 neural activity (Kato et al., 2020). Hence, it is possible that brain differences between genotype groups at the
364 start of behavioural testing, as well as a lack of activity-dependent up-regulation of oligodendrogenesis
365 triggered by exposure to the CW, might have combined to contribute to the observed behavioural
366 phenotype.

367 ***Changes in brain microstructure due to Myrf knock-out***

368 When investigating the consequences of genetic ablation of OL differentiation on brain microstructure using
369 *ex vivo* MRI, we found significantly lower MTR in multiple brain regions (Fig. 3). We hypothesised that
370 disruption of oligodendrogenesis will affect brain microstructure, as it disrupts ongoing cellular dynamics
371 and myelin formation. As MTR is related to myelin content of tissue (Lazari and Lipp, 2021), lower MTR may
372 reflect reduction in myelination caused by the significant reduction in new oligodendrocyte formation (Fig.
373 1) induced for ~5-6 weeks prior to *ex vivo* MRI. However, estimating how much myelin content was added
374 during the timeframe of interest is difficult and requires further histological investigation. Metrics derived
375 from diffusion-weighted imaging (FA, MD), that are sensitive to tissue microstructure and less sensitive or
376 specific to myelin, were not significantly affected by the deletion of *Myrf* (Suppl. Fig. 3). The finding that
377 changes in MTR were widespread across WM and GM regions is consistent with the global ablation of OL
378 differentiation across the whole CNS.

379 We found no evidence for task-dependent changes in brain microstructure related to myelination when
380 investigating how motor learning on the complex wheel affected brain microstructure (in comparison to a
381 fixed wheel control condition). Specifically, we found no effect of complex wheel running on the myelin-
382 sensitive metric MTR (Fig. 3, Suppl. Fig. 3), regardless of whether animals had disrupted oligodendrogenesis.
383 We had hypothesised that motor learning should lead to changes in myelin sensitive metrics of brain
384 microstructure if associated with increase in myelination, as previously reported in the context of the skilled
385 reaching motor learning tasks in rats (Sampaio-Baptista et al., 2013). However, there are several important
386 methodological differences between these studies, including species (rat vs mouse) and training task. The
387 reaching task involves the development of fine motor movements in comparison to the gross motor
388 movements necessary to perform the CW task. Furthermore, MRI techniques employed here can only
389 measure cellular effects very indirectly and are less sensitive to small effects compared to histological
390 approaches employed by others, which showed increased oligodendrocytes differentiation in motor cortex
391 and subcortical WM due to CW running (McKenzie et al., 2014; Xiao et al., 2016). In addition, the fixed wheel
392 control condition we employed might have offered more environmental enrichment in comparison to home
393 cage controls that are typically used. Furthermore, it is possible that at the timepoint of our measurement,
394 immediately after 12 days of training on the complex wheel, experience-induced changes in myelination
395 might not have been prominent enough to cause detectable changes in MTR. Together, we did not find
396 evidence for learning-induced changes in myelin sensitive MRI measures of brain microstructure after
397 learning to run the complex wheel.

398 ***Electrophysiological changes cause by Myrf knockout***

399 In addition to genotype differences in microstructure, deletion of *Myrf* in OPCs caused alterations in
400 oscillatory brain activity (Fig. 4), as reflected in higher EEG power density across broad frequency bands.
401 Increases in spectral power of LFPs have been reported in Plp1-KO models with mild myelin deficits (Gould et
402 al., 2018) and cuprizone models of demyelination (Dubey et al., 2022). Associated computational modelling
403 indicated that a decrease in conduction velocity, as a result of reduced myelination, can lead to an increase
404 in spectral power (Gould et al., 2018). Additionally, adaptive myelination, disrupted in P-Myrf$^{(-/-)}$ animals,
405 might regulate homeostatic coordination and oscillatory self-organization in local and large-scale brain
406 networks (Dubey et al., 2022; Noori et al., 2020; Talidou et al., 2022). Hence, it is plausible that reduced
407 myelination and disruption of adaptive myelination, caused by ablated oligodendrogenesis over a 6-7 week
408 period, led to the observed increases in EEG power density. However, identification of the underlying
409 mechanism driving such broad alterations in brain activity requires further investigation.

410 ***Summary and conclusion***

411 In summary, the findings presented in this study suggest that ablation of oligodendrogenesis by conditional
412 deletion of Myrf in PDGFa-positive OPCs leads to subtle but detectable physiological and structural
413 differences in the brain. The previously detected, and here replicated, behavioural deficit on the complex
414 running wheel might therefore partly arise as a result of these task-independent brain differences, in
415 addition to impairments in oligodendrogenesis driven by learning.

416 The current findings raise many questions for future work. For example, the timescale over which these
417 structural and physiological changes develop should be explored as we only sampled effects at a single
418 timepoint. Further, it remains to be tested whether the effects found here hold for other transgenic models
419 of disrupted oligodendrogenesis. While the use of such models has thus far been predominantly to study of
420 effects on learning, future work could investigate whether and how continuous oligodendrogenesis plays a
421 broader role in maintaining brain microstructure and function.

422 This study suggests that the implications of disrupting oligodendrogenesis in the adult mouse brain extend
423 beyond specific task-related effects and should be taken into account when interpreting behavioural
424 phenotypes and designing future experiments.

425 ***Acknowledgements***
426 The authors thank Eveliina Hanski and Luke Baxter for feedback on previous version of the manuscript. The
427 authors also want to thank Piergiorgo Salva and the entire Plasticity Group at the Wellcome Centre for
428 Integrative Neuroimaging for constructive discussions and suggestions during the project.

429 **Materials and methods**

430 ***Animals***

431 All work carried out conformed to UK Home Office legislation (Scientific Procedures Act 1986).

432 ***Mouse breeding and genetic background***

433 Mice used in this study were originally generated in the Richardson laboratory (McKenzie et al., 2014), UCL
434 by crossing *Pdgfra-CreER*^{T2} transgenic mice (Rivers et al., 2008) with Cre-conditional reporter mice *Rosa26R-*
435 *YFP* (*R26R-YFP*) (Srinivas et al., 2001) to generate double-homozygous offspring. *Cre* and *YFP* reporter lines in
436 the Richardson Laboratory were maintained separately by crossing (more than 10 generations) with C57B6
437 females (Charles River; Margate, UK). These *Pdgfra-CreER*^{T2} *:Rosa26R-YFP* were crossed with *Myrf* $^{(fl/fl)}$ mice
438 (Emery et al., 2009) to obtain *Pdgfra-CreER*^{T2}*: R26R: Myrf* $^{(+/fl)}$ offspring, which were sibling-mated to obtain
439 *Myrf* $^{(fl/fl)}$ and *Myrf* $^{(+/fl)}$ littermates. These animals were finally crossed to generate cohorts of *Pdgfra-CreER*^{T2} *:*
440 *R26R- YFP: Myrf* $^{(fl/fl)}$ and *Myrf* $^{(+/fl)}$ littermates for behavioural testing and further breeding. In the Richardson
441 Laboratory, *Myrf* $^{(fl/fl)}$ mice were obtained originally (in 2010) on a mixed 129/CBA/C57B6 background.

442 Five breeding pairs of *Pdgfra-CreER*^{T2} *: R26R- YFP: Myrf* $^{(fl/fl)}$ and *Pdgfra-CreER*^{T2} *: R26R- YFP: Myrf* $^{(+/fl)}$ (referred
443 to as P-Myrf $^{(fl/fl)}$and P-Myrf $^{(+/fl)}$) were sent to our laboratory from the Richardson Lab, UCL in 2016 and were
444 used to breed animals for our study by crossing P-Myrf $^{(fl/fl)}$ with P-Myrf $^{(+/fl)}$ mates. Mice carried copies of
445 *Pdgfra-CreER*^{T2} on both alleles and were either *R26R-YFP* $^{(+/-)}$ or *R26R-YFP* $^{(+/+)}$. Two generations of animals
446 were bred before behaviour testing started for the current studies and animals from a total of 4 consecutive
447 generations were used for behaviour testing. Hence, P-Myrf$^{(fl/fl)}$ and P-Myrf $^{(+/fl)}$ were maintained by sibling
448 crossing for 6 generations in our facilities.

449 For testing the normal and complex wheel running in wild-type mice, twenty C57BL/6JOlaHsd mice (8 males
450 and 8 females) were purchased from Envigo, UK at age P60. The mice were given a one-week period to
451 acclimate before commencing behavioural testing.

452 ***Mouse Genotyping***

453 Genotyping for Cre-ER^{T2} (Cre 5'-TCG ATG CAA CGA GTG ATG AG and Cre 3'-TTC GGC TAT ACG TAA CAG GG*;*
454 Product Size 481bp) and R26R-YFP (R26WTF1-AAA GTC GCT CTG AGT TGT TAT, R26WTR1-GGA GCG GGA
455 GAA ATG GAT ATG, R26KOF1-GCG AAG AGT TTG TCC TCA ACC) was done by PCR amplification of genomic
456 DNA. Myrf $^{(fl/fl)}$ mice were genotyped by PCR amplification of genomic DNA using primers within intron 7
457 flanking the first lox site (5'-AGGAGTGTTGTGGGAA-GTGG and 5'-CCCAGGCTGAAGATGGAATA), which gives a
458 281 bp product for the wild-type allele and a 489 bp product for the *loxP*-flanked allele (Emery et al., 2009).

459 ***Tamoxifen administration***

460 Tamoxifen (Sigma T5648) was dissolved at 40 mg/ml in corn oil on a shaker overnight at RT and by
461 subsequent sonicating at 21°C for one hour. P-Myrf $^{(+/-)}$ and P-Myrf $^{(-/-)}$ mice were generated by administering
462 tamoxifen (0.3 mg/g body weight in corn oil) by oral gavage for four consecutive days to *Pdgfra-*
463 *CreER*^{T2}*:R26R- YFP:Myrf*$^{(flox/flox)}$ and *Pdgfra-CreER*^{T2}*:R26R- YFP:Myrf*$^{(+/flox)}$. Animals were left for at least 2
464 weeks before experimental procedures. During, and for a week after tamoxifen treatment, nutritious jelly
465 and mash were provided for all mice to prevent excessive weight loss due to the adverse effects of the drug.

466 ***Behaviour testing of mice***

467 Assessment of behavioural phenotype was conducted by the same researcher. Wherever possible, equal
468 numbers of animals of each sex were included in each experimental group. For experiments for which data
469 collection was not automated, researchers were blinded to the genotype of the animals during data
470 collection and analysis. All mice were maintained on a 12-hour artificial light-dark cycle (9:00-21:00). Food
471 and water were provided *ad libitum.*

472 ***Complex running wheel***

473 Cages with running wheels were purchased from Lafayette Neuroscience (Scurry mouse mis-step wheel
474 Model 80821S). This voluntary running wheel cage comes equipped with a wheel (circumference = 0.389 m)
475 that allows individual rungs to be removed to create a complex wheel or rung configuration (Liebetanz et al.,
476 2007; McKenzie et al., 2014). The mice were provided with a "complex wheel" (CW) with 16 out of 38 rungs
477 removed to create a wheel with an irregular pattern of 22-rungs (Fig. 2A), a configuration that was adapted
478 from (McKenzie et al., 2014). For behaviour testing, mice were single caged with the running wheel, a paper
479 house filled with nesting material and wood chippings to cover the floor of the cage. Mice were accustomed
480 to the cage for 30 mins before being provided access to the running wheel by removing a dividing wall to the
481 compartment where the wheel was located. Mice were placed in the wheel cages up to 2 hours before the
482 start of the dark period. Mice ran spontaneously, without artificial reward. Food and water were available *ad*
483 *libitum* within the specialised running wheel cages.

484 Infrared sensors recorded wheel rotation, which allowed computer-controlled recording of wheel rotation as
485 a function of time for 20 cages simultaneously for 24h a day (The Scurry Activity Monitoring Software,
486 Lafayette Neuroscience, Model 86165). For data analysis, counts of full wheel rotations were exported into a
487 spreadsheet, divided into time bins of 10 seconds. Custom R scripts were used extract the following running
488 parameters from the baseline activity data: 1) distance travelled, which represents the total number of
489 wheel rotations × wheel circumference. 2) Active intervals, which represent the number of 10 second
490 intervals in which at least one full wheel rotation was recorded. 3) Average speed, which represents the sum

491 of the distance run divided by the number of active intervals. 4) Maximum speed, which was calculated by
492 determining the average speed in the 1% of fastest intervals run. Analysis of performance was conducted for
493 either chronological time intervals (length of time vector) or for intervals of time that animals spent running
494 on the wheel (length of vector containing only active intervals on the wheel).

495 Running speed of animals (distance/time) was conducted using time bins of 10 seconds. McKenzie *et al.*
496 (2014) calculated the average running speed by quantifying wheel spins during a 1 min time bin. Yet, in the
497 current study between 35-40% of continuous running bouts were found to be shorter than 1 minute long
498 (data not shown). That meant that average running speed was often not accurately estimated when using 1
499 min intervals to calculate speed. Hence, 10 sec bins were chosen for this study.

500 ***Complex running wheel and fixed wheel testing for ex vivo MRI experiment***

501 A total of 24 animals were tested on the complex running wheel (P-Myrf$^{(+/-)}$:n=12, 5 females; P-Myrf$^{(-/-)}$:n=12,
502 4 females) in specific running wheel cages as described above. Additionally, 25 littermates were exposed to a
503 static fixed complex wheel that was not able to rotate (referred to as fixed wheel, FW) in cages with
504 otherwise identical set up (P-Myrf$^{(+/-)}$:n=12, 4 females; P-Myrf$^{(-/-)}$:n=13, 5 females). As the fixed wheel had the
505 same missing rungs pattern that allows animals to pass between rungs, animals could climb and interact
506 with the wheel as a kind of environmental enrichment yet could not run and turn the wheel. The experiment
507 consisted of 5 distinct batches of P-Myrf animals bred from the same set of 5 breeding pairs over
508 consecutive litters. Littermates were semi-randomly assigned to cages equipped with either a complex
509 wheel (CW) or a fixed wheel (FW) and were tested in the same environment and timeframe. Semi-random
510 assignment meant that animals were randomly assigned to a wheel type, while attempting to balance the
511 numbers of genotype, sex and littermates equally between experimental groups.

512 ***Accelerating RotaRod***

513 Mice were tested on a standard RotaRod apparatus (Ugo Basile, Italy). Mice were tested for their ability to
514 stay on a rod 3 cm in dimeter (Suppl. Fig. 1 B). The apparatus allowed simultaneous testing of up to 5 mice,
515 yet a maximum of 3 mice were tested at the same time. Mice were habituated to the testing room for 30
516 mins before behaviour testing, by placing their cages into the room. Mice were trained for three trials on the
517 rotarod at a constant speed (4 rpm), 120 s each trial, 2 days before behaviour testing, at which speed all
518 mice stayed on the rod for the duration of the trial.

519 On the day of testing, each mouse was held by the tail and allowed to grasp the rotating rod. If it was still in
520 place after 10 s, then the rotation of the rod was accelerated by 20 rpm to a maximum speed of 40 rpm. The
521 time at which each mouse fell off the rod was recorded, starting from the moment of acceleration. If a
522 mouse managed to stay on the rod for longer than 150 s, the trial was stopped, and a time of 150 s was

523 recorded. Each mouse was tested 3 times on the same day. Animals were allowed to rest for 10 minutes
524 between trials.

525 ***Balance beam***

526 The beam apparatus consists of 1 meter round smooth wooden beams of 15 mm or 7.5 mm diameter
527 positioned 50 cm above the table. A soft foam matt was placed beneath the beam to cushion any potential
528 fall. The beam rested on the edge of a wooden box on one side, at which animals were placed for testing. On
529 the other side, the beam rested on the edge of the animal's home cage (Suppl. Fig. 1C). The beam was
530 slightly angled (~10 degrees) so that animals had to walk uphill to reach their home cage. A lamp (with a 60-
531 watt light bulb) was used to shine light above the start point and serve as an aversive stimulus, and the light
532 inside the room was slightly dimmed. Mice were habituated to the testing room for 1 hour before behaviour
533 testing, by placing their cage inside the room. Three days before behaviour assessment on the balance
534 beam, mice were trained to cross the beam. Training was done by placing the mice on the beam (1.5 cm
535 diameter) opposite the home cage. During training mice were freely allowed to cross the beam and reach
536 their home cage. This procedure was repeated 3 times with a 1-min rest time between attempts. Training
537 was conducted as almost all mice stopped on the beam or tried to turn around in the middle during the first
538 exposure to the apparatus. Only after learning the location of their home cage during training do the mice
539 reliably cross the beam without stopping and turning around, which allows reliable and comparable data
540 collection. All mice successfully crossed the beams during training at least one time.

541 For testing, mice were placed on the beam and freely allowed to cross the beam. Mice were first tested on
542 the wider beam (1.5 cm diameter). After a 5-min resting time in the home cage, the beam was exchanged for
543 the narrow (0.75 cm diameter) beam and the same animal was tested again. All animals successfully crossed
544 the beams without falling. The apparatus was cleaned with ethanol (70%) before testing another animal.

545 Testing was recorded using an HD camera placed on the side of the beam opposite the home cage. Videos
546 were analysed by a blinded experimenter. Foot slips (defined as the foot coming off the top of the beam)
547 and the number of steps taken to cross the beam were quantified.

548 ***Perfusion of animals and tissue processing***

549 Animals were deeply anaesthetized (Euthatal: 80mg/kg, i.p) with sodium pentobarbital and transcardially
550 perfused with 10 ml PBS, followed by 30 ml paraformaldehyde (4% w/v in 0.1 M phosphate buffer) with the
551 help of a perfusion pump (Flow rate: 4ml/min). After perfusion, animal skulls were dissected by removing
552 soft tissue from the outside of the skull (skin, muscle, eyes, etc.) and the lower jaws. Dissected skulls
553 containing the CNS tissue were stored overnight in 4% PFA at 4°C for 24h. Samples were then washed with
554 phosphate buffer saline (PBS) before being stored in PBS at 4°C. Samples were sent to the Center for Image

555 Sciences, UMCU, Utrecht, Netherlands for magnetic resonance imaging (MRI). After MR imaging, tissue
556 samples were sent back to the University of Oxford, cryoprotected with 30% sucrose solution, embedded in
557 OCT and stored at -80°C until processed for histological analysis.

558 ***Immunohistochemistry of free-floating brain sections***

559 For Immunohistochemical analysis, coronal cryosections (30 µm) were cut (anterior to posterior) from the
560 first section at which the anterior corpus callosum was visible and continuously connected from one
561 hemisphere to the other. Brain sections were collected and washed in Tris-buffered Saline (TBS; Sigma) and
562 processed as floating sections. All incubations and washes were performed on a shaker at 60 rpm. Sections
563 were blocked in TBS containing 10% Normal Goat Serum (Sigma), 0.5% Triton-X (Sigma) and 1% BSA for 2
564 hours at room temperature. The primary antibodies used were anti-PDGF-Ra (rabbit, New England Biolabs,
565 1:400 dilution), anti-APC (clone CC1; mouse, Calbiochem, 1:200 dilution) and/or anti-GFP(YFP) (chicken,
566 Avas, 1:500), which were diluted in TBS containing 10% of the blocking solution (see above) at 4°C. Samples
567 were then incubated with corresponding fluorophore conjugated secondary antibodies (1:500, Alexa FluorO-
568 488 or 546, Thermo Fischer Scientific), diluted in blocking solution (1:10) for 2h at room temperature.
569 Samples were mounted and dried for ~10 mins before being sealed under a glass cover with Vectorshield
570 anti-fade mounting medium (Vectorshield laboratories) and viewed by a Zeiss L subse SM-700 confocal
571 microscope and ZEN software. Cells were counted in low-magnification photo-micrographs (x20 objective) of
572 non-overlapping fields of coronal sections (320mmx320mm each) of the corpus callosum, between the
573 dorsolateral corners of the lateral ventricles (6 fields per section, three sections per animal), as illustrated in
574 Suppl. Fig. 6. The surface area of corpus callosum was calculated for each animal to determine cellular
575 density. Image analysis was performed using Fuji/ImageJ (NIH).

576 ***Statistical analysis of histological and behavioural data***

577 ***Criteria for excluding animals from complex wheel data analysis***

578 Previous experiments reveal that a small subset of healthy untreated animals show unusually low
579 engagement in voluntary wheel running. To prevent such outliners from skewing overall group performance,
580 we set the following pre-determined exclusion criteria for analysis of complex wheel behaviour
581 performance: animals were excluded from the analysis if: 1) they ran less than 1km in 8 Days (P-Myrf$^{(+/-)}$;
582 n=4, females; P-Myrf$^{(-/-)}$; n=1), or 2) ran less than 100 meters per day for at least half of the days recorded (P-
583 Myrf$^{(+/-)}$; n=2, females; P-Myrf$^{(-/-)}$; n=1). In total, that led to the exclusion of 8 animals based on these criteria
584 (P-Myrf$^{(+/-)}$; n=6; P-Myrf$^{(-/-)}$; n=2).

585 ***Testing for the effect of covariates on complex wheel running***

586 Before analysing the effect of genotype on behaviour, we assessed whether a number of different covariates
587 might influence our findings, in order to determine which covariates to include in subsequent analyses. First,
588 to test for a potential effect of the generations and sex on the performance on the CW, a mixed two-way
589 ANOVA (within subject factor: days (over 8 days of running); between subject factors: sex, generation) was
590 used to analyse daily running speed (average or maximum). This analysis revealed that sex, but not
591 generation, had a significant effect maximum running speeds (sex: $F(1,116)=22.68$, $p<0.001$) on the complex
592 wheel, with females consistently outperforming males (Suppl. Fig. 1G). Apart from consistently running
593 longer distances on the CW (total distance in m: female, M±SD=35505±22374; males, M±SD=16413±14426),
594 females also spent more time on the CW than males over a period of 8 consecutive days (Suppl. Fig. 1H).
595 While there was an expected difference in body weight between sexes, there was no difference in body
596 weight between P-Myrf$^{(-/-)}$ and P-Myrf$^{(+/-)}$ animals for either sex at the start of behaviour testing (body
597 weight in g: male-Myrf$^{(+/)}$, M±SD=24.1±3.4; male-Myrf$^{(-/-)}$, M±SD=24.3±2.4; female-Myrf$^{(+/-)}$,
598 M±SD=19.7.1±1.4, female-Myrf$^{(-/-)}$, M±SD=19.4±2.3).

599 The main analysis of behavioural performance on the CW combines data from several experiments. Hence,
600 the age of tamoxifen treatment (range: P58-93, M±SD=77.11±8.6), the age at behaviour testing (range: P92-
601 135, M±SD=109.9±7.9) and the days between tamoxifen treatment and behaviour testing (range: P21-43,
602 M±SD=32.8±7.5) varied between animals, experiments and generations (Suppl. Table 1). However, we found
603 no statistically significant correlation between the performance of the P-Myrf$^{(-/-)}$ on the CW (average running
604 speed) and any of the age parameters mentioned above in the compiled data set of all P-Myrf animals. Yet, it
605 is of note that our experiments were not specifically designed to compare the effect of these age parameters
606 on running performance.

607 In summary, of the potential covariates tested, only sex was found to be significantly associated with running
608 behaviour and so this factor was included as a fixed factor in all subsequent analyses of genotype differences
609 to control for the induced variability.

610 ***Statistical analysis method***

611 Statistical analysis was performed using R (R Core Team, 2021), using he rstatix (0.7.0; Kassambara, 2021)
612 and the psycho (v0.6.2; Makowski, 2021) packages. The statistical tests used for a particular analysis are
613 mentioned during the data presentation in the result sections. Normality of the data and assumptions of
614 homogeneity of variance were tested (e.g. with Levene's Test) before using parametric statistical analysis. If
615 these assumptions were not met, non-parametric alternative tests were used for statistical analysis, or the
616 test parameters were adjusted to account for the lack of homogeneity of variances (e.g. using un-pooled
617 variances and a correction to the degrees of freedom for unpaired t-test) whenever possible.

618 Performance on the complex wheel was analysed using a mixed two-way ANOVAs. However, sample data
619 did not always meet the assumption of normality due to a tendency towards bimodal distribution in the
620 sample population. Despite this we proceeded to apply ANOVA as I) this statistical analysis shows a certain
621 robustness to type 1 error due to moderate violation of assumptions of normality at the range of sample
622 sizes used in this study (Arnau et al., 2013; Blanca et al., 2018, 2017), II) no ideal alternative non-parametric
623 statistical analysis exist for a mixed model ANOVA, and III) the same statistical analysis was used for the data
624 set that we are attempting to replicate. If the assumption of sphericity (Mauchly's Test) was violated in the
625 mixed two-way ANOVA, Greenhouse-Geisser procedures were used to estimate epsilon in order to correct
626 the degrees of freedom of the F-distribution. In this case, adjusted degrees of freedom are presented.
627 Asterisks are used to indicate statistical significance when appropriate: *=p<0.05, **=p<0.01 ***=p<0.001.
628 Details of statistical analysis approaches and results for each dataset are provided in Suppl. Table 2

629 ***MRI methods***

630 ***MRI acquisition***

631 Post-mortem high-resolution structural MRI was performed on a 9.4 T horizontal bore MR system (Varian,
632 Palo Alto, CA, USA) at the Center for Image Sciences, UMCU, Utrecht, Netherlands, equipped with a 6 cm ID
633 gradient insert with gradients up to 1 T/m. A custom-made solenoid coil with an internal diameter of 2.6 cm
634 was used for excitation and reception of the MR signal. Three perfusion-fixed brains were inserted with the
635 skulls intact in a custom-made holder and immersed in non-magnetic oil (Fomblin, Solvay Solexis).

636 Diffusion weighted imaging (DWI) was acquired with 3D eight shot spin-echo EPI sequence with the
637 following parameters: 60 diffusion encoding directions; 1 average per image; 5 images with no diffusion
638 weighting; TR/TE 500/38.6 ms, field of view: 24x20x20 mm; isotropic resolution of 0.125 mm ; δ/Δ 5.5/8.91
639 ms, diffusion gradient strength (half-sine shape) 73 G/cm, b = 3522 s/mm2; total acquisition time 12.3 hrs.

640 Magnetization transfer images were also acquired with a 3D eight shot spin-echo EPI sequence with a train
641 of saturating pulses in front of the image acquisition saturating frequencies 5 kHz, 10 kHz, and 100 kHz off
642 resonance. Four volumes per frequency offset were acquired (TR/TE 500/28ms; field of view: 24x20x20 mm;
643 resolution of 0.125 mm isotropic; total time 2.3 hrs).

644 A total of 71 animals were scanned for *ex vivo* MRI. Unfortunately, a subset of 20 animals were perfused by a
645 different experimenter using a different perfusion method. Due to complications with the perfusion method
646 and a significant deviation in measured MRI metrics from the remaining cohort, these 20 samples had to be
647 excluded from the analysis.

MRI data processing

All data were Fourier transformed and combined using home-written software in MatLab (Mathworks®) from the Dijkhuizen lab, UMCU, Utrecht, Netherlands. These scripts can be provided on request. DWI data were analysed with the FMRIB Diffusion Toolbox. Voxel-wise values of fractional anisotropy (FA) and mean diffusivity (MD) were estimated from the original DWI data using 'dtifit'.

For alignment of the images to the same space, individual brain images were digitally separated from the triplets in which they were acquired. For the optimal registration of images in grey and white matter, two different contrasts were combined (both weighted equally): i) FA and ii) and mean of all diffusion weighted directions. A study specific template of all subject images was then acquired using an automated image registration pipeline as described previously (Lerch et al., 2011, 2008). In short, this approach brings all scans into anatomical alignment in an automated and unbiased fashion using a combination of mni_autoreg tools (Collins et al., 1994) and Advanced Normalization Tools (ANTS) (Avants et al., 2008). FSL (for FMRIB Software Library) tools, version 6.0 (www.fmrib.ox.ac.uk/fsl) were used for linear (FLIRT) and nonlinear transformations (FNIRT) to the study specific template (Scripts can be provided on request). Transformations gained from this approach were applied to the individual modalities of interest (FA, MD, MTR).

White matter structures were analysed using a modified version of Tract-Based Spatial Statistics (TBSS; Smith et al., 2006). The skeleton for TBSS was thresholded at an FA value of 0.28 as to reliably contain major tracts in the mouse brain that can be accurately aligned across individuals. Finally, the FA values of the tract centers (i.e., maximum FA values) were projected onto the skeleton for each mouse brain and fed into statistical analysis. MD and MTR values for the same voxels were also projected into the skeleton.

MRI data analysis

For region of interest **(ROI)** analysis, an aggregate atlas combining 182 individually segmented structures (Dorr et al., 2008; Richards et al., 2011; Steadman et al., 2014; Ullmann et al., 2013) was registered to the unbiased consensus average of the current study (the atlas is available at http://repo.mouseimaging.ca/repo/DSURQE_40micron_nifti/) and masks for the specific ROI (M1, M2, S1, Hippocampus) were extracted from the atlas. Mean values from each ROI for each subject were extracted for statistical analysis in R studio. Mixed ANOVAs were used for group comparison. where regions of Interest (ROIs) were within subject factors and genotype and/or wheel were between subject factors. As data was collected from 4 consecutive experimental groups, experimental group (n=4) was included as a fixed factor to control for introduced variability. Significant effects in within-subject factor (ROIs) were followed by a post-hoc simple comparison between groups (wheel or genotype), Bonferroni adjusted for number of ROIs. Statistical analysis was performed using R (R Core Team, 2021), using he rstatix (0.7.0; Kassambara, 2021). To check for outliers, mean values for each metric were extracted from the whole brain mask and checked for extreme outliers ('*identify_outliers*',

681 *rstatix* package, R). One animal (P-Myrf$^{(-/-)}$, CW) was identified as an extreme outlier and subsequently re-
682 moved from the ROI analysis. Statistical analysis including the outlier are provided in Suppl Table 2.
683
684 For voxel-wise analysis across the whole brain, nonparametric permutation testing with a cluster-forming
685 threshold of $t > 2$ and 5000 permutations were used to determine corrected p values. Clusters with a
686 corrected significance of $p < 0.05$ were deemed significant. We tested for differences between the genotype
687 groups (Myrf$^{(-/-)}$ vs Myrf$^{(+/-)}$, wheel type (complex wheel vs fixed wheel) and for a genotype*wheel type
688 interaction (Scripts and GLMs can be provided on request). We also tested for voxel-wise for correlations
689 between contrast and wheel performance (maximum speed, total distance).

690 Finally, to test for global effects, we calculate mean values for each MR metric across all voxels within the
691 GM mask or the WM skeleton.

692 ***EEG methods***

693 ***Electrophysiology data collection***

694 Chronic electrophysiological recordings were undertaken in seven male adult mice (P-Myrf $^{(-/-)}$: n=4; P-Myrf
695 $^{(+/-)}$: n=3). All mice received tamoxifen at age P75 and were implanted at ages P110-120, and the reported
696 recordings were collected at age P130. The animals were surgically implanted with a custom-made
697 headstage tethered to electrodes for the continuous recording of electroencephalogram (EEG) and
698 electromyogram (EMG). EEG screw electrodes (Fine Science Tools) were inserted into the skull. 5 electrodes
699 were implanted in total: above the right and left frontal cortex (primary motor area: anteroposterior +2 mm,
700 mediolateral +2 mm), above the right and left occipital cortex (primary visual area: anteroposterior +3.5 mm,
701 mediolateral +2.5 mm), and above the cerebellum (which served as a reference). As per Fisher *et al.*, 2016),
702 two custom-soldered stainless steel wires were inserted into the right and left nuchal muscles respectively,
703 for the recording of EMG. A schematic diagram of implantation locations is shown in Fig. 4A.
704
705 Immediately before surgery, analgesics were administered (subcutaneous injection of 1–2 mg/kg metacam
706 and 0.08 mg/kg vetergesic). Isoflurane was used for induction and maintenance of anesthesia throughout
707 the surgical procedure (4% and 1–2% respectively). After surgery, analgesics were given for at least 3 days
708 (1–2 mg/kg oral metacam) and animal wellbeing was closely monitored for 1-2 weeks, until the animal
709 returned to baseline conditions. All procedures were performed under a UK Home Office Project License and
710 conformed to the Animal Scientific Procedures Act 1986.
711
712 Two animals were implanted each day, with all surgeries taking place in the same week. Order of surgery
713 was randomised to ensure balanced allocation of genotype to time of day of surgery (i.e. morning surgery vs

afternoon surgery) and to time of week surgery (i.e. early in the week or late in the week), to avoid systemic bias in implantations and in length of time elapsed between implantation and recording.

Electrophysiology data processing

Data acquisition was performed using the Multichannel Neurophysiology Recording System (TDT, Alachua FL, USA). EEG/EMG data were filtered between 0.1–100 Hz, amplified (PZ5 NeuroDigitizer pre-amplifier, TDT Alachua FL, USA) and stored on a local computer at a sampling rate of 256.9 Hz. EEG/EMG data were resampled offline at a sampling rate of 256 Hz. Signal conversion was performed using custom-written Matlab (The MathWorks Inc, Natick, Massachusetts, USA) scripts and was then transformed into European Data Format (Fisher et al., 2016). Custom MATLAB scripts were used to estimate the power spectral density using the multitaper method ("pmtm()" function , Signal Processing Toolbox, Matlab) for 4-s epochs f. A 0.25 Hz resolution was used for plotting of EEG power density across frequency bands. Total power within the 1-30hz range across the frontal and occipital channel was calculated and compared using ANOVAs for repeated measures (Within-Subject Factor: Location; Between Subject Factor: Genotype). Peak frequency was defined as the frequency bin (0.25 Hz resolution) with the highest power. Power within specific frequency bands was calculated and compared between genotype groups: delta, δ (0.5–3 Hz), theta, θ (4–12 Hz), beta, β (12.5–25 Hz), and gamma, γ (30–80 Hz). Statistical analysis was performed using R (R Core Team, 2021), using he rstatix (0.7.0; Kassambara, 2021).

Scoring and analysis of vigilance states

Recordings were quality-checked during acquisition. All data was manually scored by a blinded investigator (S.R.) for vigilance states, as previously described in Fisher et al. (2016). Briefly, waking was defined based on a low-amplitude fast-frequency EEG activity and high EMG amplitude, NREM sleep was characterised by the predominance of slow waves and sleep spindles on the EEG and low EMG tone, while REM sleep was characterised by strong theta EEG activity, especially in the occipital derivation and low EMG activity. To validate scoring accuracy, a subset of the data was re-scored by another investigator (A.L.). Scoring quality was further verified by a third investigator (V.V.). The channel of the left hemisphere was selected for group comparison, unless a blinded investigator (V.V.) indicated that the quality of the data was significantly better in the right hemisphere, in which case the right hemisphere channel was used.

744 **References**

745 Arnau, J., Bendayan, R., Blanca, M.J., Bono, R., 2013. The effect of skewness and kurtosis on the robustness
746 of linear mixed models. Behav. Res. Methods 45, 873–879. https://doi.org/10.3758/s13428-012-
747 0306-x
748 Bacmeister, C.M., Huang, R., Osso, L.A., Thornton, M.A., Conant, L., Chavez, A., Poleg-Polsky, A., Hughes,
749 E.G., 2022. Motor Learning Drives Dynamic Patterns of Intermittent Myelination on Learning-
750 activated Axons. https://doi.org/10.1101/2021.10.13.464319
751 Bergles, D.E., Richardson, W.D., 2016. Oligodendrocyte Development and Plasticity. Cold Spring Harb.
752 Perspect. Biol. 8, a020453. https://doi.org/10.1101/cshperspect.a020453
753 Blanca, M.J., Alarcón, R., Arnau, J., Bono, R., Bendayan, R., 2018. Effect of variance ratio on ANOVA
754 robustness: Might 1.5 be the limit? Behav. Res. Methods 50, 937–962.
755 https://doi.org/10.3758/s13428-017-0918-2
756 Blanca, M.J., Alarcón, R., Arnau, J., Bono, R., Bendayan, R., 2017. Non-normal data: Is ANOVA still a valid
757 option? Psicothema 29, 552–557. https://doi.org/10.7334/psicothema2016.383
758 Bonetto, G., Belin, D., Káradóttir, R.T., 2021. Myelin: A gatekeeper of activity-dependent circuit plasticity?
759 Science 374, eaba6905. https://doi.org/10.1126/science.aba6905
760 Cullen, C.L., Pepper, R.E., Clutterbuck, M.T., Pitman, K.A., Oorschot, V., Auderset, L., Tang, A.D., Ramm, G.,
761 Emery, B., Rodger, J., Jolivet, R.B., Young, K.M., 2021. Periaxonal and nodal plasticities modulate
762 action potential conduction in the adult mouse brain. Cell Rep. 34, 108641.
763 https://doi.org/10.1016/j.celrep.2020.108641
764 Dawson, M.R.L., Polito, A., Levine, J.M., Reynolds, R., 2003. NG2-expressing glial progenitor cells: an
765 abundant and widespread population of cycling cells in the adult rat CNS. Mol. Cell. Neurosci. 24,
766 476–488. https://doi.org/10.1016/s1044-7431(03)00210-0
767 Dorr, A.E., Lerch, J.P., Spring, S., Kabani, N., Henkelman, R.M., 2008. High resolution three-dimensional brain
768 atlas using an average magnetic resonance image of 40 adult C57Bl/6J mice. NeuroImage 42, 60–69.
769 https://doi.org/10.1016/j.neuroimage.2008.03.037
770 Dubey, M., Pascual-Garcia, M., Helmes, K., Wever, D.D., Hamada, M.S., Kushner, S.A., Kole, M.H.P., 2022.
771 Myelination synchronizes cortical oscillations by consolidating parvalbumin-mediated phasic
772 inhibition. eLife 11, e73827. https://doi.org/10.7554/eLife.73827
773 Emery, B., Agalliu, D., Cahoy, J.D., Watkins, T.A., Dugas, J.C., Mulinyawe, S.B., Ibrahim, A., Ligon, K.L.,
774 Rowitch, D.H., Barres, B.A., 2009. Myelin gene regulatory factor is a critical transcriptional regulator
775 required for CNS myelination. Cell 138, 172–185. https://doi.org/10.1016/j.cell.2009.04.031
776 Fisher, S.P., Cui, N., McKillop, L.E., Gemignani, J., Bannerman, D.M., Oliver, P.L., Peirson, S.N., Vyazovskiy,
777 V.V., 2016. Stereotypic wheel running decreases cortical activity in mice. Nat. Commun. 7, 13138.
778 https://doi.org/10.1038/ncomms13138
779 Foster, A.Y., Bujalka, H., Emery, B., 2019. Axoglial interactions in myelin plasticity: Evaluating the relationship
780 between neuronal activity and oligodendrocyte dynamics. Glia 67, 2038–2049.
781 https://doi.org/10.1002/glia.23629
782 Geraghty, A.C., Gibson, E.M., Ghanem, R.A., Greene, J.J., Ocampo, A., Goldstein, A.K., Ni, L., Yang, T., Marton,
783 R.M., Paşca, S.P., Greenberg, M.E., Longo, F.M., Monje, M., 2019. Loss of Adaptive Myelination
784 Contributes to Methotrexate Chemotherapy-Related Cognitive Impairment. Neuron 103, 250-
785 265.e8. https://doi.org/10.1016/j.neuron.2019.04.032
786 Gibson, E.M., Purger, D., Mount, C.W., Goldstein, A.K., Lin, G.L., Wood, L.S., Inema, I., Miller, S.E., Bieri, G.,
787 Zuchero, J.B., Barres, B.A., Woo, P.J., Vogel, H., Monje, M., 2014. Neuronal activity promotes
788 oligodendrogenesis and adaptive myelination in the mammalian brain. Science 344, 1252304.
789 https://doi.org/10.1126/science.1252304
790 Gould, E.A., Busquet, N., Shepherd, D., Dietz, R.M., Herson, P.S., Simoes de Souza, F.M., Li, A., George, N.M.,
791 Restrepo, D., Macklin, W.B., 2018. Mild myelin disruption elicits early alteration in behavior and
792 proliferation in the subventricular zone. eLife 7, e34783. https://doi.org/10.7554/eLife.34783

793 Hibbits, N., Pannu, R., John Wu, T., Armstrong, R.C., 2009. Cuprizone demyelination of the corpus callosum in
794 mice correlates with altered social interaction and impaired bilateral sensorimotor coordination.
795 ASN NEURO 1, e00013. https://doi.org/10.1042/AN20090032
796 Hill, R.A., Li, A.M., Grutzendler, J., 2018. Lifelong cortical myelin plasticity and age-related degeneration in
797 the live mammalian brain. Nat. Neurosci. 21, 683–695. https://doi.org/10.1038/s41593-018-0120-6
798 Hughes, E.G., Orthmann-Murphy, J.L., Langseth, A.J., Bergles, D.E., 2018. Myelin remodeling through
799 experience-dependent oligodendrogenesis in the adult somatosensory cortex. Nat. Neurosci. 21,
800 696–706. https://doi.org/10.1038/s41593-018-0121-5
801 Kaller, M.S., Lazari, A., Blanco-Duque, C., Sampaio-Baptista, C., Johansen-Berg, H., 2017. Myelin plasticity and
802 behaviour-connecting the dots. Curr. Opin. Neurobiol. 47, 86–92.
803 https://doi.org/10.1016/j.conb.2017.09.014
804 Kassambara, A., 2023. rstatix: Pipe-Friendly Framework for Basic Statistical Tests.
805 Kato, D., Wake, H., Lee, P.R., Tachibana, Y., Ono, R., Sugio, S., Tsuji, Y., Tanaka, Y.H., Tanaka, Y.R., Masamizu,
806 Y., Hira, R., Moorhouse, A.J., Tamamaki, N., Ikenaka, K., Matsukawa, N., Fields, R.D., Nabekura, J.,
807 Matsuzaki, M., 2020. Motor learning requires myelination to reduce asynchrony and spontaneity in
808 neural activity. Glia 68, 193–210. https://doi.org/10.1002/glia.23713
809 Knowles, J.K., Batra, A., Xu, H., Monje, M., 2022. Adaptive and maladaptive myelination in health and
810 disease. Nat. Rev. Neurol. 18, 735–746. https://doi.org/10.1038/s41582-022-00737-3
811 Lakhani, B., Borich, M.R., Jackson, J.N., Wadden, K.P., Peters, S., Villamayor, A., MacKay, A.L., Vavasour, I.M.,
812 Rauscher, A., Boyd, L.A., 2016. Motor Skill Acquisition Promotes Human Brain Myelin Plasticity.
813 Neural Plast. 2016, 7526135. https://doi.org/10.1155/2016/7526135
814 Lazari, A., Lipp, I., 2021. Can MRI measure myelin? Systematic review, qualitative assessment, and meta-
815 analysis of studies validating microstructural imaging with myelin histology. NeuroImage 230,
816 117744. https://doi.org/10.1016/j.neuroimage.2021.117744
817 Liebetanz, D., Baier, P.C., Paulus, W., Meuer, K., Bähr, M., Weishaupt, J.H., 2007. A highly sensitive
818 automated complex running wheel test to detect latent motor deficits in the mouse MPTP model of
819 Parkinson's disease. Exp. Neurol. 205, 207–213. https://doi.org/10.1016/j.expneurol.2007.01.030
820 McKenzie, I.A., Ohayon, D., Li, H., de Faria, J.P., Emery, B., Tohyama, K., Richardson, W.D., 2014. Motor skill
821 learning requires active central myelination. Science 346, 318–322.
822 https://doi.org/10.1126/science.1254960
823 Micheva, K.D., Wolman, D., Mensh, B.D., Pax, E., Buchanan, J., Smith, S.J., Bock, D.D., 2016. A large fraction
824 of neocortical myelin ensheathes axons of local inhibitory neurons. eLife 5, e15784.
825 https://doi.org/10.7554/eLife.15784
826 Mitew, S., Gobius, I., Fenlon, L.R., McDougall, S.J., Hawkes, D., Xing, Y.L., Bujalka, H., Gundlach, A.L., Richards,
827 L.J., Kilpatrick, T.J., Merson, T.D., Emery, B., 2018. Pharmacogenetic stimulation of neuronal activity
828 increases myelination in an axon-specific manner. Nat. Commun. 9, 306.
829 https://doi.org/10.1038/s41467-017-02719-2
830 Nave, K.-A., 2010. Myelination and support of axonal integrity by glia. Nature 468, 244–252.
831 https://doi.org/10.1038/nature09614
832 Noori, R., Park, D., Griffiths, J.D., Bells, S., Frankland, P.W., Mabbott, D., Lefebvre, J., 2020. Activity-
833 dependent myelination: A glial mechanism of oscillatory self-organization in large-scale brain
834 networks. Proc. Natl. Acad. Sci. 117, 13227–13237. https://doi.org/10.1073/pnas.1916646117
835 Pajevic, S., Basser, P.J., Fields, R.D., 2014. Role of myelin plasticity in oscillations and synchrony of neuronal
836 activity. Neuroscience 276, 135–147. https://doi.org/10.1016/j.neuroscience.2013.11.007
837 Pajevic, S., Plenz, D., Basser, P.J., Fields, R.D., 2022. Oligodendrocyte-mediated Myelin Plasticity and its role
838 in Neural Synchronization. https://doi.org/10.1101/2022.07.03.498570
839 Pan, S., Mayoral, S.R., Choi, H.S., Chan, J.R., Kheirbek, M.A., 2020. Preservation of a remote fear memory
840 requires new myelin formation. Nat. Neurosci. 23, 487–499. https://doi.org/10.1038/s41593-019-
841 0582-1
842 Richards, K., Watson, C., Buckley, R.F., Kurniawan, N.D., Yang, Z., Keller, M.D., Beare, R., Bartlett, P.F., Egan,
843 G.F., Galloway, G.J., Paxinos, G., Petrou, S., Reutens, D.C., 2011. Segmentation of the mouse

844 hippocampal formation in magnetic resonance images. NeuroImage 58, 732–740.
845 https://doi.org/10.1016/j.neuroimage.2011.06.025
846 Rivers, L.E., Young, K.M., Rizzi, M., Jamen, F., Psachoulia, K., Wade, A., Kessaris, N., Richardson, W.D., 2008.
847 PDGFRA/NG2 glia generate myelinating oligodendrocytes and piriform projection neurons in adult
848 mice. Nat. Neurosci. 11, 1392–1401. https://doi.org/10.1038/nn.2220
849 Salzer, J.L., Zalc, B., 2016. Myelination. Curr. Biol. CB 26, R971–R975.
850 https://doi.org/10.1016/j.cub.2016.07.074
851 Sampaio-Baptista, C., Johansen-Berg, H., 2017. White Matter Plasticity in the Adult Brain. Neuron 96, 1239–
852 1251. https://doi.org/10.1016/j.neuron.2017.11.026
853 Sampaio-Baptista, C., Khrapitchev, A.A., Foxley, S., Schlagheck, T., Scholz, J., Jbabdi, S., DeLuca, G.C., Miller,
854 K.L., Taylor, A., Thomas, N., Kleim, J., Sibson, N.R., Bannerman, D., Johansen-Berg, H., 2013. Motor
855 skill learning induces changes in white matter microstructure and myelination. J. Neurosci. Off. J.
856 Soc. Neurosci. 33, 19499–19503. https://doi.org/10.1523/JNEUROSCI.3048-13.2013
857 Sampaio-Baptista, C., Vallès, A., Khrapitchev, A.A., Akkermans, G., Winkler, A.M., Foxley, S., Sibson, N.R.,
858 Roberts, M., Miller, K., Diamond, M.E., Martens, G.J.M., De Weerd, P., Johansen-Berg, H., 2020.
859 White matter structure and myelin-related gene expression alterations with experience in adult rats.
860 Prog. Neurobiol. 187, 101770. https://doi.org/10.1016/j.pneurobio.2020.101770
861 Schalomon, P.M., Wahlsten, D., 2002. Wheel running behavior is impaired by both surgical section and
862 genetic absence of the mouse corpus callosum. Brain Res. Bull. 57, 27–33.
863 https://doi.org/10.1016/S0361-9230(01)00633-5
864 Scholz, J., Klein, M.C., Behrens, T.E.J., Johansen-Berg, H., 2009. Training induces changes in white-matter
865 architecture. Nat. Neurosci. 12, 1370–1371. https://doi.org/10.1038/nn.2412
866 Shimizu, T., Nayar, S.G., Swire, M., Jiang, Y., Grist, M., Bannerman, D.M., Johansen-Berg, H., Ogasawara, K.,
867 Tohyama, K., Richardson, W.D., 2023. Oligodendrocyte dynamics dictate individual performance
868 outcomes of working memory training in mice. https://doi.org/10.1101/2023.01.17.524381
869 Smith, S.M., Jenkinson, M., Johansen-Berg, H., Rueckert, D., Nichols, T.E., Mackay, C.E., Watkins, K.E.,
870 Ciccarelli, O., Cader, M.Z., Matthews, P.M., Behrens, T.E.J., 2006. Tract-based spatial statistics:
871 voxelwise analysis of multi-subject diffusion data. NeuroImage 31, 1487–1505.
872 https://doi.org/10.1016/j.neuroimage.2006.02.024
873 Srinivas, S., Watanabe, T., Lin, C.-S., William, C.M., Tanabe, Y., Jessell, T.M., Costantini, F., 2001. Cre reporter
874 strains produced by targeted insertion of EYFP and ECFP into the ROSA26 locus. BMC Dev. Biol. 1, 4.
875 https://doi.org/10.1186/1471-213X-1-4
876 Steadman, P.E., Ellegood, J., Szulc, K.U., Turnbull, D.H., Joyner, A.L., Henkelman, R.M., Lerch, J.P., 2014.
877 Genetic effects on cerebellar structure across mouse models of autism using a magnetic resonance
878 imaging atlas. Autism Res. 7, 124–137. https://doi.org/10.1002/aur.1344
879 Steadman, P.E., Xia, F., Ahmed, M., Mocle, A.J., Penning, A.R.A., Geraghty, A.C., Steenland, H.W., Monje, M.,
880 Josselyn, S.A., Frankland, P.W., 2020. Disruption of Oligodendrogenesis Impairs Memory
881 Consolidation in Adult Mice. Neuron 105, 150-164.e6. https://doi.org/10.1016/j.neuron.2019.10.013
882 Talidou, A., Frankland, P.W., Mabbott, D., Lefebvre, J., 2022. Homeostatic coordination and up-regulation of
883 neural activity by activity-dependent myelination. Nat. Comput. Sci. 1–12.
884 https://doi.org/10.1038/s43588-022-00315-z
885 Ullmann, J.F.P., Watson, C., Janke, A.L., Kurniawan, N.D., Reutens, D.C., 2013. A segmentation protocol and
886 MRI atlas of the C57BL/6J mouse neocortex. NeuroImage 78, 196–203.
887 https://doi.org/10.1016/j.neuroimage.2013.04.008
888 Xiao, L., Ohayon, D., McKenzie, I.A., Sinclair-Wilson, A., Wright, J.L., Fudge, A.D., Emery, B., Li, H., Richardson,
889 W.D., 2016. Rapid production of new oligodendrocytes is required in the earliest stages of motor-
890 skill learning. Nat. Neurosci. 19, 1210–1217. https://doi.org/10.1038/nn.4351
891 Xin, W., Chan, J.R., 2020. Myelin plasticity: sculpting circuits in learning and memory. Nat. Rev. Neurosci. 21,
892 682–694. https://doi.org/10.1038/s41583-020-00379-8

Yalçın, B., Pomrenze, M.B., Malacon, K., Chau, I.J., Taylor, K.R., Ni, L., Contreras-Esquivel, D., Malenka, R.C., Monje, M., 2022. Myelin plasticity in ventral tegmental area is required for opioid reward. https://doi.org/10.1101/2022.09.01.506263

Young, K.M., Psachoulia, K., Tripathi, R.B., Dunn, S.-J., Cossell, L., Attwell, D., Tohyama, K., Richardson, W.D., 2013. Oligodendrocyte Dynamics in the Healthy Adult CNS: Evidence for Myelin Remodeling. Neuron 77, 873–885. https://doi.org/10.1016/j.neuron.2013.01.006

Zatorre, R.J., Fields, R.D., Johansen-Berg, H., 2012. Plasticity in gray and white: neuroimaging changes in brain structure during learning. Nat. Neurosci. 15, 528–536. https://doi.org/10.1038/nn.3045

Supplementary Material

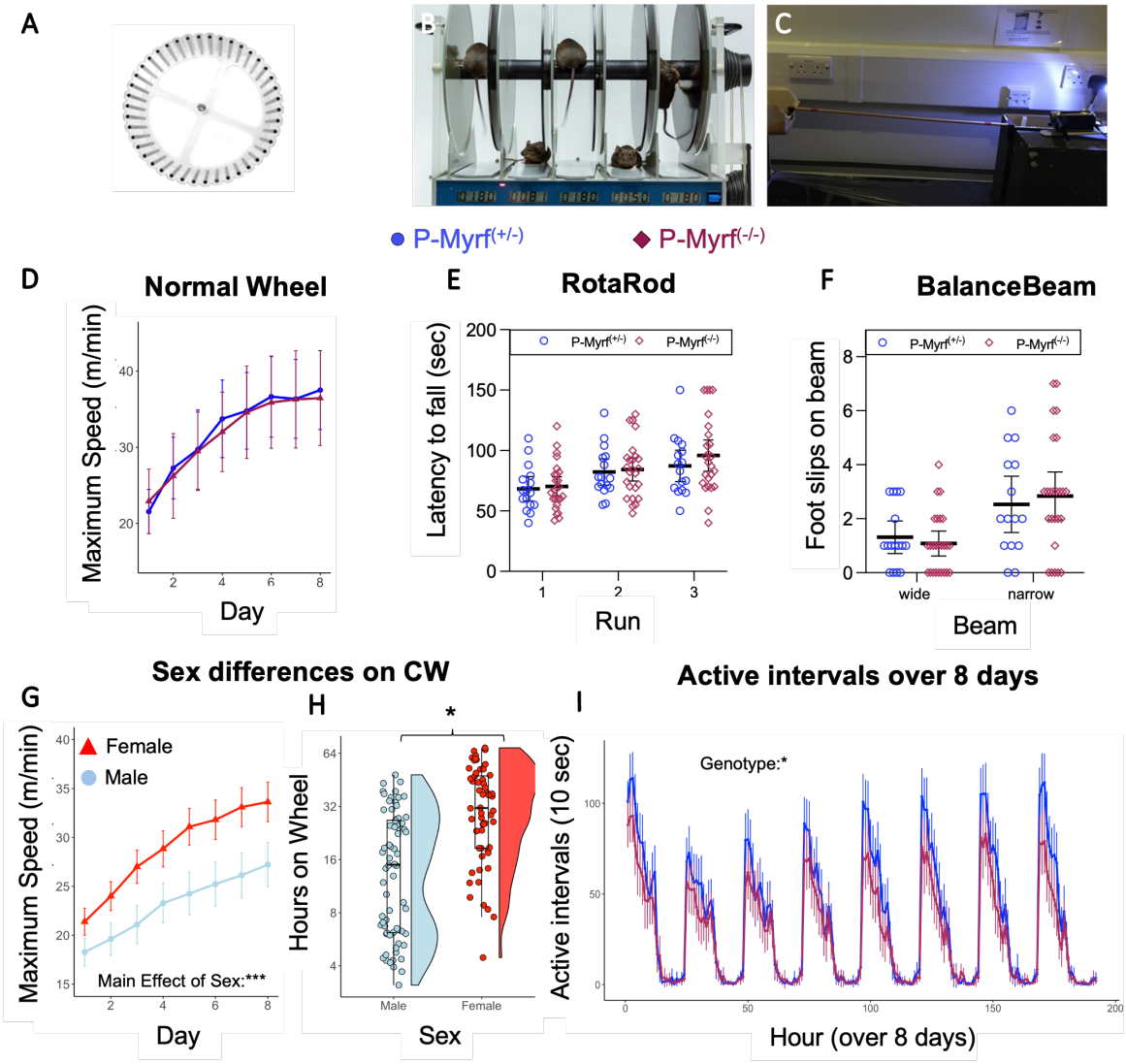

Suppl. Fig. 1. ***Control task for motor behaviour and supplementary data for the complex running wheel data. (A)*** *To test general performance on a running wheel, a cohort of P-Myrf(-/-) and P-Myrf(+/-) animals were tested on a normal wheel which had none of the rungs removed. To test for general motor ability and coordination, a cohort of animals was tested on the (B) RotaRod and (C) Balance Beam task. (D) Conditional knockout of Myrf did not affect performance on a normal running wheel (P-Myrf(+/-); n=17; P-Myrf(-/-); n=18) , nor did it lead to a difference in performance on the (E) RotaRod or (F) Balance Beam tasks (P-Myrf(+/-); n=16, P-Myrf(-/-); n=25) which may have indicated a more general motor skill deficit. (G-H) Sex difference in running speed and activity level. (G) Females (n=57) outperformed males (n=67) on the complex running wheel in terms of running performance (Mixed ANOVA: Main effect of Sex; F(1,120)= 19.98, p<0.001). (H) Females also spent more time active on the wheel over 8 days Mann-Whitney U, p=0.014. (K) Active intervals over 8 days (1 hour time bins) for P-Myrf(-/-) and P-Myrf(+/-) animals. While both Genotypes displayed comparable day/night activity patterns, P-Myrf(-/-) had on average fewer active intervals on the CW during the night when compared to P-Myrf(+/-) (Mixed ANOVA: Main effect of Genotype: (F(1,120)=4.48 p=036). Data presented as Mean ± 95%CI. Data presented as Mean±95%CI or boxplots. Asterix indicate statistical significance (*p<0.05, **p<0.01, ***p<0.001).*

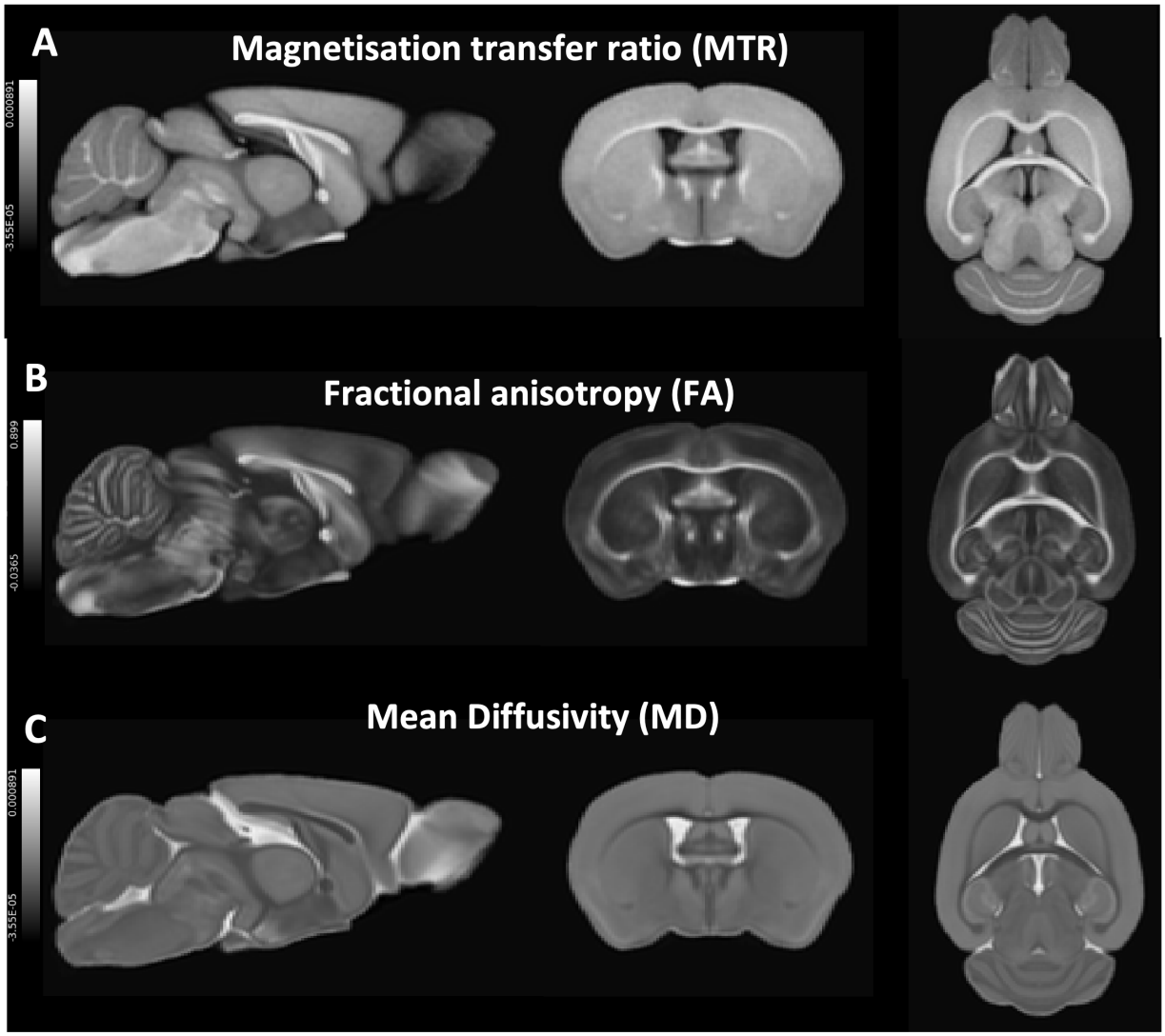

Suppl. Fig. 2. ***Example images for different parameter contrasts extracted from ex vivo MRI for quantification of brain microstructure.*** *Brain microstructure was assessed using a 9.4 T horizontal bore MR scanner (Varian, Palo Alto, CA, USA)* ***(A)*** *Magnetisation transfer ratio (MTR) allows indirect detection of water bound to macromolecules, such as lipids and proteins, and is thus sensitive to myelin (Deloire-Grassin et al. 2000).* ***(B)*** *Fractional anisotropy (FA) describes the anisotropy of diffusion of water molecules.* ***(C)*** *Mean Diffusivity (MD), which describes the rotationally invariant magnitude of water diffusion within brain tissue. Images shown are the mean of all individual subject images analysed for this study.*

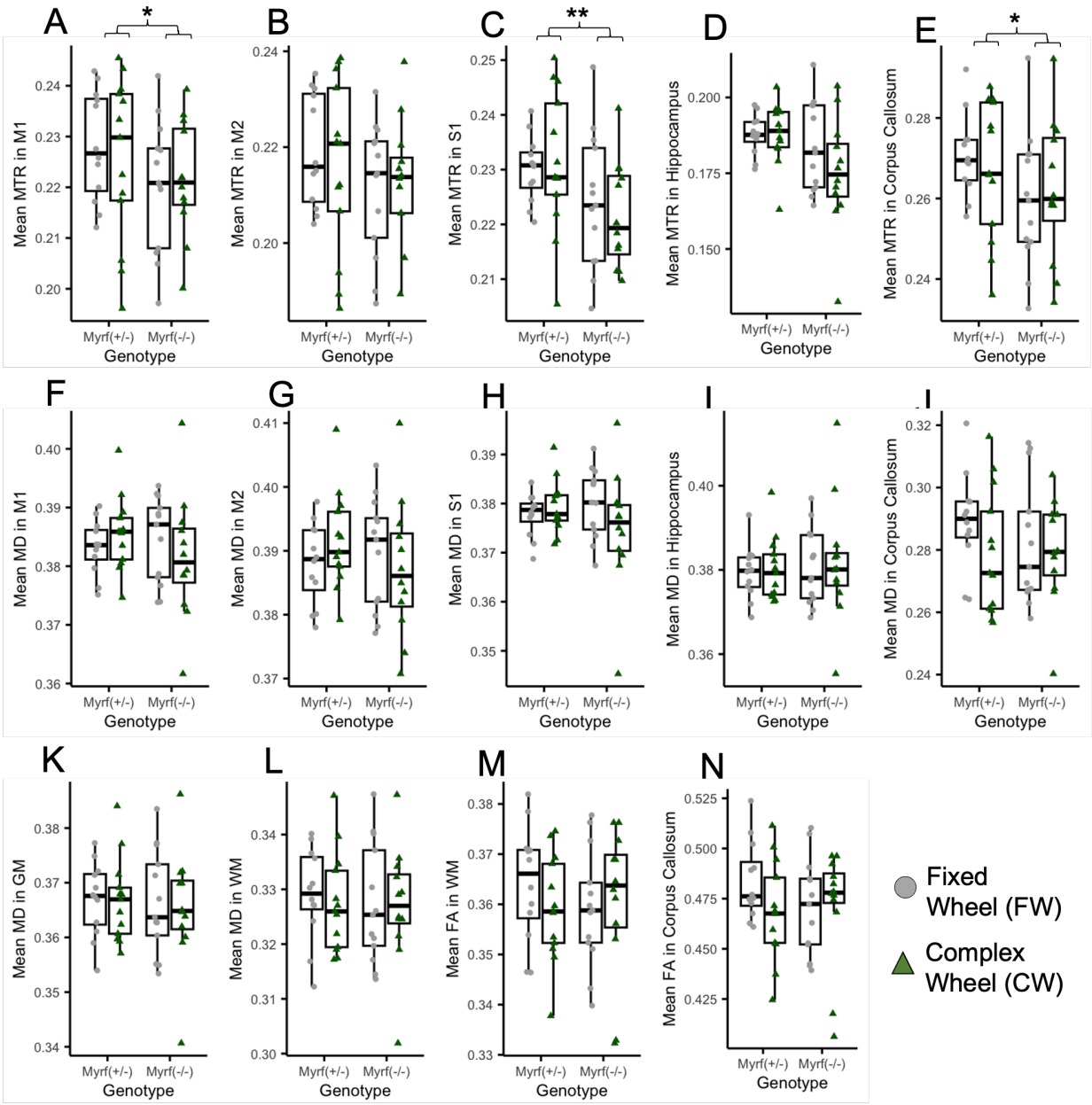

Suppl. Fig. 3. ***Region of Interest (ROI) Analysis of brain microstructure, as measure by MTR, MD and FA. (A-E)*** *MTR values in grey matter ROIs. A Mixed ANOVA revealed a main effect of Genotype in MTR grey matter regions, post-hoc pairwise comparison (Bonferroni adjusted) revealed a significant Genotype effect in the* ***(A)*** *Primary motor cortex (M1),* ***(C)*** *Somatosensory Cortex (S1), and* ***(E)*** *MTR in the anterior Corpus Callosum.* ***(F-J)*** *DWI-derived Mean Diffusivity (MD) values in ROI,* ***(K)*** *whole brain mask and* ***(L)*** *white ma_tter skeleton.* ***(M-N)*** *DWI-derived Fractional Anisotropy (FA) values in* ***(M)*** *white matter skeleton and* ***(N)*** *anterior corpus callosum. Asterix indicate statistical significance (*p<0.05, **p<0.01).*

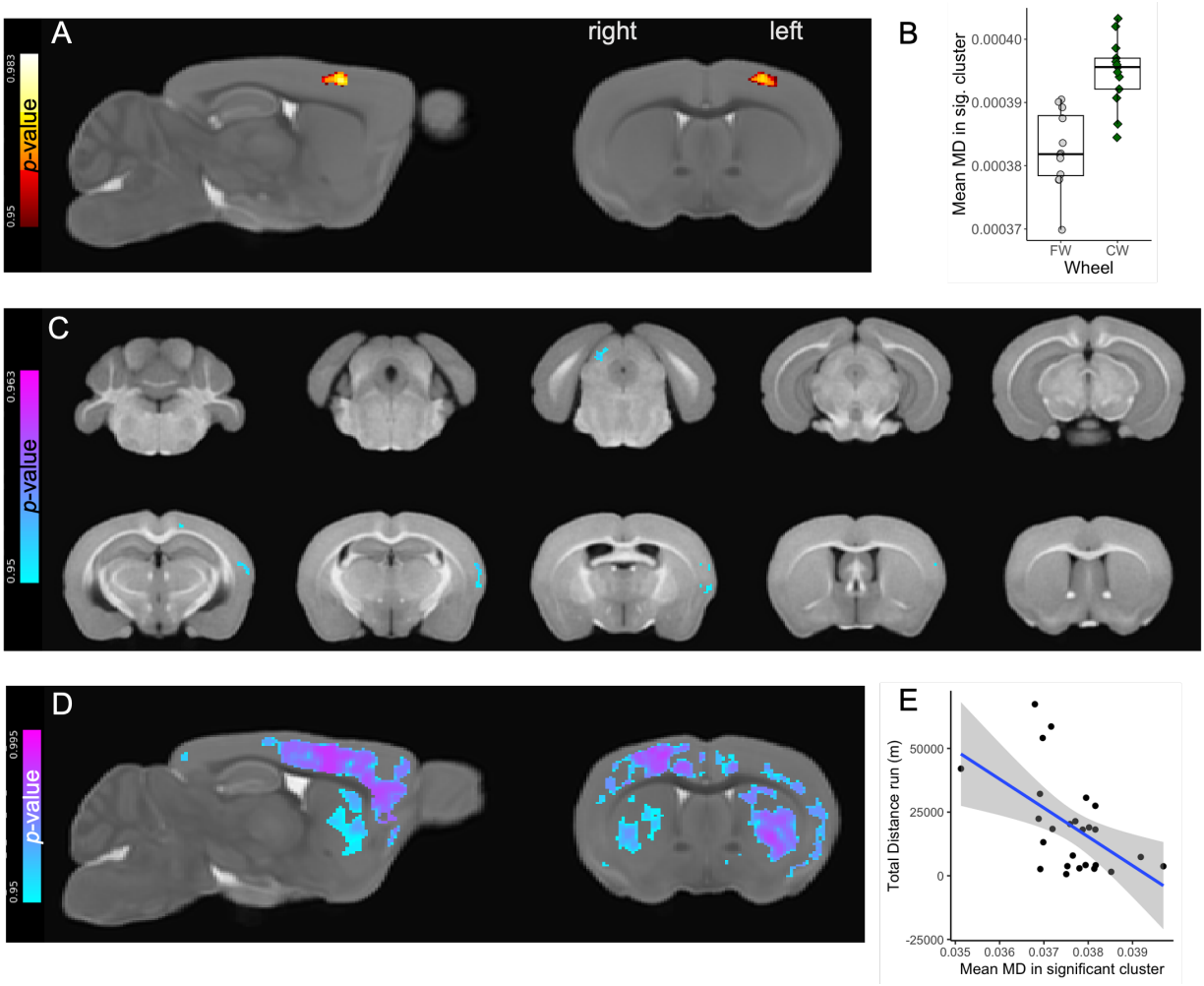

Suppl. Fig. 4. ***Voxel-wise analysis of DWI-derived parameters revealed an effect wheel running in brain microstructure.*** *Results from Voxel-wise analysis of MRI-derived metrics. (**A**) A cluster in the right primary motor cortex (M1) grey matter region had higher MD for P-Myrf$^{(-/+)}$ control animals that ran on the Complex Wheel (CW), when compared to P-Myrf$^{(-/+)}$ exposed to the fixed wheel (FW). (**B**) Mean MD extracted from cluster depicted in (**A**). **(C)** MTR was lower for P-Myrf$^{(-/-)}$ animals in a few clusters located in cortical regions and the midbrain (superior colliculus). (**D**) MD across a diffuse area across the grey matter was correlated to the total distance ran on the complex running wheel by animals across both genotypes. **(E)** Mean MD extracted from the ROI depicted in **(D)** plotted against the total distance run on the complex wheel. Permutation test ('randomise', FSL) used for voxel-wise analysis. Spearman's test used for correlation analysis.*

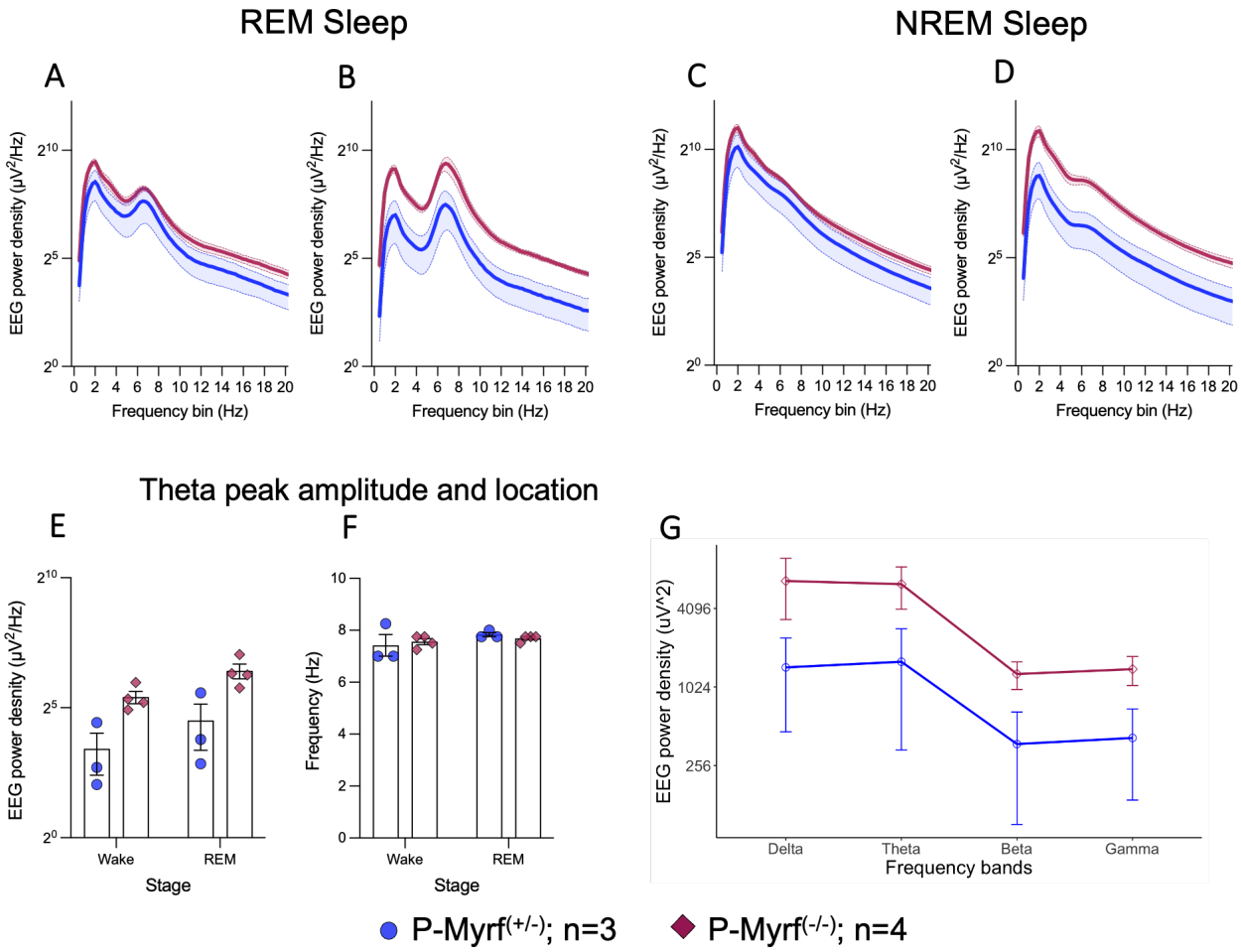

Suppl. Fig. 5. ***Difference in EEG recording between P-Myrf$^{(-/-)}$ and P-Myrf$^{(+/-)}$.*** *EEG power density by frequency during rapid eye movement (REM) sleep in* ***(A)*** *frontal channel and* ***(B)*** *occipital channels. EEG power density by frequency during non-REM sleep (NREM) in* ***(C)*** *frontal channel and* ***(D)*** *occipital channels.* ***(E)*** *Amplitude and* ***(F)*** *location of peak theta power per vigilance state (Wake, REM) as measured in occipital channel. While peak amplitude was different between the genotype groups, there was no shift in the frequency of the peak.* ***(G)*** *Mean group EEG power density (PSD) per frequency bands, delta, δ (0.5–3 Hz), theta, ϑ (4–12 Hz), beta, β (12.5–25 Hz), and gamma, γ (30-60 Hz). Data presented as Mean±SEM.*

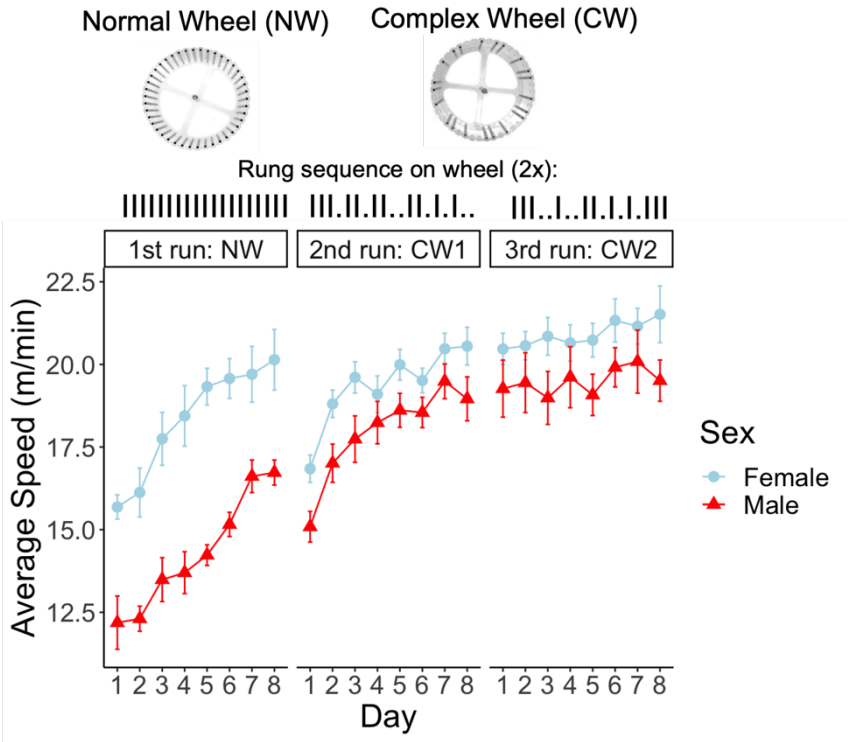

Suppl. Fig. 6. ***The effect of complex wheel sequence on running performance.*** *Wildtype mice (C58BL/6JOIaHsd, 8 females, 8 males, Age: P84) exposed to a normal running wheel (NW) show significant improvements in their running speed over 8 days (Main effect of Day: $F(3.14, 47.1)=21.8$, $p<0.001$), with females outperforming males (Sex*Day Interaction: $F(1, 15)=34.6$, $p<0.001$). Switching to complex running wheel (CW1) leads to a temporary reduction in running speed (Day 8 on NW vs Day 1 on CW1; Main effect of wheel: $F(1, 14)=27.0$, $p<0.001$) , indicating a specific task demand of the complex wheel. However, running speed on day 1 on CW1 is significantly higher than on day 1 on NW (Main effect of wheel: $F(1, 14)=12.0$, $p=0.004$), indicating some skill in wheel running was retained between NW and CW1. Switching the rung sequence of the complex running wheel (CW2) after 8 days has no effect on running performance compared to last day of running on CW1. Mixed Two-way ANOVA used for statistical analysis (between-subject factor: Sex; within-subject factor: Time (8 Levels) or Wheel (2 Levels)). Data presented as Mean±SEM.*

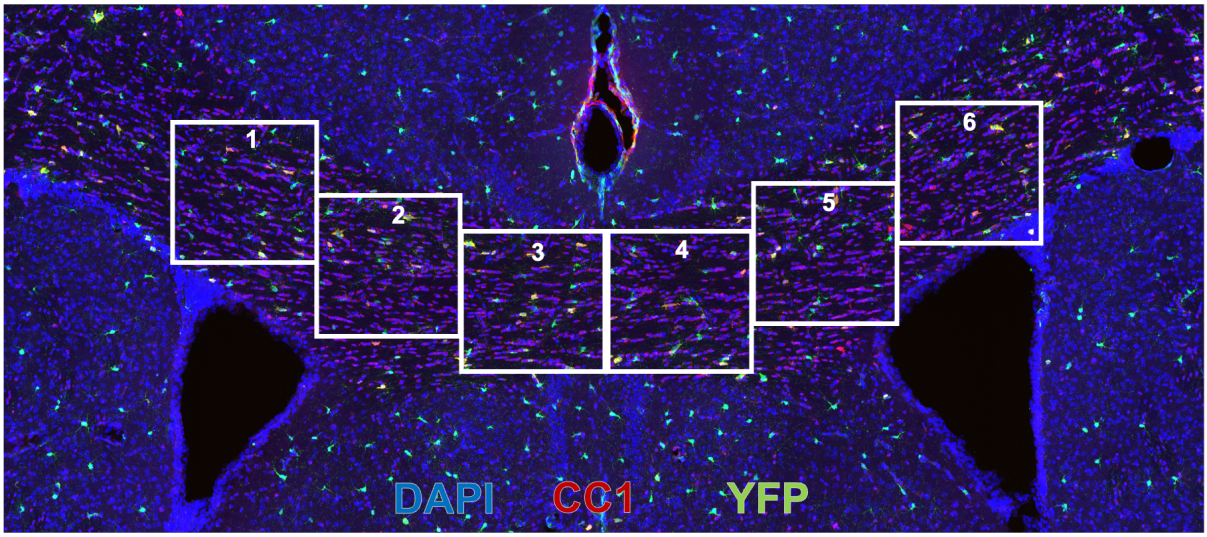

Suppl. Fig. 7. ***Quantification of oligodendrocyte differentiation in the corpus Callosum*** *Representative image of a brain slices showing the anterior Corpus Callosum region used for quantification of YFP+ positive OPCs and CC1+ mature Oligodendrocytes. Six images were taken from each section (three sections per animal), as illustrated by the white frames in the image.*

.035

.036

.037 *Suppl. Table 1.* ***Variability of animal's age at important experimental timepoints within different***

.038 ***generations of Myrf-cKO animals that ran the complex wheel.*** *Age is presented in days after birth*

Generation	Number of Animals	Age at tamoxifen treatment	Age between tamoxifen treatment and CW	Age at beginning of CW testing	Experiments / Data
G1	17 P-Myrf$^{(-/+)}$ = 7 P-Myrf$^{(-/-)}$ = 10	Range=69-84 Mean=73.5 SD=4.1	Range=31-42 Mean=36.5 SD=5.5	Range=100-126 Mean=109.8 SD=6.8	Complex Wheel (8 days)
G2	19 P-Myrf$^{(-/+)}$ = 11 P-Myrf$^{(-/-)}$ = 8	Range=58-93 Mean=74.6 SD=13.9	Range=34-42 Mean=38.1 SD=4.1	Range=92-135 Mean=112.4 SD=17.1	Complex Wheel (8 days)
G3	39 P-Myrf$^{(-/+)}$ = 15 P-Myrf$^{(-/-)}$ = 24	Range=64-83 Mean=71.4 SD=5.9	Range=30-43 Mean=37.8 SD=5.9	Range=96-114 Mean=109.14 SD=4.8	Complex Wheel (8 days) Followed by: RotaRod & Balance Beam
G4	49 P-Myrf$^{(-/+)}$ = 26 P-Myrf$^{(-/-)}$ = 23	Range=79-88 Mean=83.8 SD=2.3	Range=21-30 Mean=25.4 SD=2.9	Range=102-116 Mean=109.1 SD=2.9	Complex Wheel (12 days) Ex vivo MRI Histology

.039

.040

.041

.042

.043

.044

.045

.046

.047

.048

.049

.050

.051

.052

Suppl. Table 2: ***Comprehensive information on the statistical analysis methods utilized and the corresponding results for each dataset.***

Figure	Data & Methods	Statistical results				
Fig. 1C	Welch's t-test. P-Myrf(+/-), n=12; P-Myrf(-/-), n=15.	YFP+ cells: t = 4.5627, df = 15.462, p-value = 0.000347 YFP+CC1+: t = 7.1621, df = 11.274, p-value = 1.61e-05 YFP+CC1-: t = 0.72468, df = 24.246, p-value = 0.4756				
Fig. 1D	Welch's t-test. P-Myrf(+/-), n=12; P-Myrf(-/-), n=15.	YFP+CC1+/YFP+CC1-: t = 10.199, df = 11.338, p-value = 4.706e-07				
Fig. 2D	Mixed Two-way ANOVA P-Myrf(+/-), n=59 (Female, n=28); P-Myrf(-/-), n=65 (Female, n=29); Between subject factor: MYRFGenotype (2 levels), Sex (2 levels) Within subject factor: Time (Days, 8 levels)	**Effect**	**DFn**	**DFd**	**F**	**p**
		(Intercept)	1	120	900.615	<0.001
		MYRFGenotype	1	120	10	0.002
		Sex	1	120	13.081	<0.001
		Time	2.74	328.53	170.149	<0.001
		MYRFGenotype:Sex	1	120	3.041	0.084
		MYRFGenotype:Time	2.74	328.53	5.569	0.001
		Sex:Time	2.74	328.53	6.344	<0.001
Fig. 2E	Mixed Two-way ANOVA P-Myrf(+/-), n=59 (Female, n=28); P-Myrf(-/-), n=65 (Female, n=29); Between subject factor: MYRFGenotype (2 levels), Sex (2 levels) Within subject factor: Time (Days, 8 levels)	**Effect**	**DFn**	**DFd**	**F**	**p**
		(Intercept)	1	120	1791.129	<0.001
		MYRFGenotype	1	120	11.922	<0.001
		Sex	1	120	17.481	<0.001
		Time	2.57	308.96	185.786	<0.001
		MYRFGenotype:Sex	1	120	1.867	0.174
		MYRFGenotype:Time	2.57	308.96	4.764	0.005
		Sex:Time	2.57	308.96	4.614	0.006
Fig. 2F	Mann–Whitney U test P-Myrf(+/-), n=59 (Female, n=28); P-Myrf(-/-), n=65 (Female, n=29);	W = 2504, p-value = 0.003369				
Fig. 2G	Mann–Whitney U test P-Myrf(+/-), n=59 (Female, n=28); P-Myrf(-/-), n=65 (Female, n=29);	W = 2536, p-value = 0.001988				
Fig. 2H	Mixed Two-way ANOVA P-Myrf(+/-), n=59 (Female, n=28); P-Myrf(-/-), n=65 (Female, n=29); Between subject factor: MYRFGenotype (2 levels), Sex (2 levels) Within subject factor: Time (12 levels (20 mins intervals))	**Effect**	**DFn**	**DFd**	**F**	**p**
		MYRFGenotype	1	120	2.727	0.101
		Sex	1	120	0.753	0.387
		Time	4.83	579.63	62.791	<0.001
		MYRFGenotype:Sex	1	120	5.446	0.021
		MYRFGenotype:Time	4.83	579.63	2.627	0.025
		Sex:Time	4.83	579.63	3.088	0.01
Fig. 2I	Mann–Whitney U test P-Myrf(+/-), n=59 (Female, n=28); P-Myrf(-/-), n=65 (Female, n=29);	W = 2413.5, p-value = 0.01317				
Fig. 2J	Mann–Whitney U test P-Myrf(+/-), n=59 (Female, n=28); P-Myrf(-/-), n=65 (Female, n=29);	W = 2411, p-value = 0.01364				
Fig. 2K	Spearman's rank correlation rho:	Across Genotype: S = 63551, p-value <0.001, rho = 0.7999962 P-Myrf(+/−): S = 12760, p-value <0.001, rho 0.6271278 P-Myrf(-/−): S = 5874.6, p-value <0.001, rho 0.8716223				

	cor.test(a, b method=c("spearman")) P-Myrf(+/-), n=59 (Female, n=28); P-Myrf(-/-), n=65 (Female, n=29);					
Fig. 2L	Mixed Two-way ANOVA P-Myrf(+/-), n=59 (Female, n=28); P-Myrf(-/-), n=64 (Female, n=29); Between subject factor: MYRFGenotype (2 Levels), Sex (2 Levels) Within subject factor: Time (6 levels (10 mins intervals))	**Effect**	**DFn**	**DFd**	**F**	**p**
		MYRFGenotype	1	120	2.848	0.094
		Sex	1	120	0.058	0.81
		Time	2.21	265.32	88.001	<0.001
		MYRFGenotype:Sex	1	120	2.846	0.094
		MYRFGenotype:Time	2.21	265.32	9.06	<0.001
		Sex:Time	2.21	265.32	1.81	0.161
Fig. 2M	Mann–Whitney U test P-Myrf(+/-), n=59 (Female, n=28); P-Myrf(-/-), n=65 (Female, n=29);	W = 2490, p-value = 0.00421				
Fig. 2N	Mixed Two-way ANOVA P-Myrf(+/-), n=59 (Female, n=28); P-Myrf(-/-), n=64 (Female, n=29); Between subject factor: MYRFGenotype (2 Levels), Sex (2 Levels) Within subject factor: Time (5 Intervals (1H intervals))	**Effect**	**DFn**	**DFd**	**F**	**p**
		MYRFGenotype	1	118	4.998	0.027
		Sex	1	118	3.09	0.081
		Time	2.2	259.93	53.822	<0.001
		MYRFGenotype:Sex	1	118	3.709	0.057
		MYRFGenotype:Time	2.2	259.93	1.224	0.298
		Sex:Time	2.2	259.93	3.045	0.044
Fig. 2O	Mann–Whitney U test P-Myrf(+/-), n=58 (Female, n=28); P-Myrf(-/-), n=64 (Female, n=29);	W = 2278, p-value = 0.0307				
Fig. 3D	Mixed Two-way ANOVA P-Myrf(+/-), n=12 P-Myrf(-/-), n=13 Between subject factor: MYRFGenotype (2 Levels), Batch (4 Levels) Within subject factor: ROI (4 Levels)	**Effect**	**DFn**	**DFd**	**F**	**p**
		MYRFGenotype	1	17	7.318	0.015
		Batch	3	17	0.889	0.467
		ROI	1.27	21.57	190.596	<0.001
		MYRFGenotype:Batch	3	17	2.786	0.072
		MYRFGenotype:ROI	1.27	21.57	2.084	0.161
		Batch:ROI	3.81	21.57	3.034	0.041
Fig. 3D	Two-way ANOVAs P-Myrf(+/-), n=12 P-Myrf(-/-), n=13 Between subject factor: MYRFGenotype (2 Levels), Batch (4 Levels)	**ROI**	**Effect**	**F**	**p**	**p (adjusted)**
		MTRHipp	MYRFGenotype	0.969	0.339	1
		MTRM1	MYRFGenotype	10.523	0.005	0.02
		MTRM2	MYRFGenotype	9.029	0.008	0.032
		MTRS1	MYRFGenotype	5.224	0.035	0.14
Fig. 3E	Two-way ANOVA P-Myrf(+/-), n=12 P-Myrf(-/-), n=13 Between subject factor: MYRFGenotype (2 Levels), Batch (4 Levels)	**ROI**	**DFn**	**DFd**	**F**	**p**
		MTRaCCWMskel	1	17	7.77	0.013
Fig. 3G	Grey matter skeleton - MTR Two-way ANOVA P-Myrf(+/-), n=25 P-Myrf(-/-), n=25 Between subject factor: MYRFGenotype (2 Levels), Batch (4 Levels)	Effect	DFn	DFd	F	p
		MYRFGenotype	1	34	6.04	0.019
		Wheel	1	34	0.065	0.8
		Batch	3	34	2.179	0.108
		MYRFGenotype:Wheel	1	34	0.061	0.807
		MYRFGenotype:Batch	3	34	1.117	0.356

		Wheel:Batch	3	34	0.395	0.758
Fig. 3H	White matter skeleton - MTR Two-way ANOVA P-Myrf(+/-), n=25 P-Myrf(-/-), n=25 Between subject factor: MYRFGenotype (2 Levels), Wheel (2 Levels), Batch (4 Levels)	**Effect**	**DFn**	**DFd**	**F**	**p**
		MYRFGenotype	1	34	4.728	0.037
		Wheel	1	34	0.028	0.869
		Batch	3	34	1.563	0.216
		MYRFGenotype:Wheel	1	34	0.083	0.775
		MYRFGenotype:Batch	3	34	0.939	0.433
		Wheel:Batch	3	34	0.697	0.56
Fig. 4E	Mixed Two-way ANOVA P-Myrf(+/-), n=3 P-Myrf(-/-), n=4 Between subject factor: MYRFGenotype (2 Levels), Within subject factor: EEG location (2 Levels)	**Effect**	**DFn**	**DFd**	**F**	**p**
		Genotype	1	5	10.398	0.023
		EEG location	1	5	4.207	0.096
		Genotype: EEG location	1	5	0.779	0.418
Fig. 4F	Mixed Two-way ANOVA P-Myrf(+/-), n=3 P-Myrf(-/-), n=4 Between subject factor: MYRFGenotype (2 Levels), Within subject factor: EEG location (2 Levels)	**Effect**	**DFn**	**DFd**	**F**	**p**
		Genotype	1	5	12.751	0.016
		EEG location	1	5	0.155	0.71
		Genotype: EEG location	1	5	1.463	0.28
Fig. 4H	Mixed Two-way ANOVA P-Myrf(+/-), n=3 P-Myrf(-/-), n=4 Between subject factor: MYRFGenotype (2 Levels), Within subject factor: EEG location (2 Levels)	**Effect**	**DFn**	**DFd**	**F**	**p**
		Genotype	1	5	11.385	0.02
		EEG location	1	5	1.762	0.242
		Genotype:EEG location	1	5	1.071	0.348
Suppl. Fig. 1H	Mann–Whitney U test Males: n=67; Females: n=57;	W = 2411, p-value = 0.01364				
Suppl. Fig 1I	Mixed Two-way ANOVA P-Myrf(+/-), n=59 (Female, n=28); P-Myrf(-/-), n=64 (Female, n=29); Between subject factor: MYRFGenotype (2 Levels), Sex (2 Levels) Within subject factor: Time (192 Intervals – 1h size))	**Effect**	**DFn**	**DFd**	**F**	**p**
		MYRFGenotype	1	120	4.484	0.036
		Sex	1	120	30.276	<0.001
		Interval	191	22920	103.115	<0.001
		MYRFGenotype:Sex	1	120	0.604	0.438
		MYRFGenotype:Interval	191	22920	2.12	<0.001
		Sex:Interval	191	22920	8.859	<0.001
Suppl. Fig 3A-D	Mixed Two-way ANOVA P-Myrf(+/-), n=25 P-Myrf(-/-), n=25 Between subject factor: MYRFGenotype (2 Levels), Batch (4 Levels) Within subject factor: ROI (4 Levels)	**Effect**	**DFn**	**DFd**	**F**	**p**
		MYRFGenotype	1	34	10.464	0.003
		Wheel	1	34	0.196	0.661
		Batch	3	34	3.426	0.028
		ROI_GM_MTR	1.27	43.21	299.344	<0.001
		MYRFGenotype:Wheel	1	34	0.076	0.784
		MYRFGenotype:Batch	3	34	2.39	0.086
		Wheel:Batch	3	34	0.455	0.715
		MYRFGenotype:ROI_GM_MTR	1.27	43.21	0.196	0.719
		Wheel:ROI_GM_MTR	1.27	43.21	0.34	0.615
Suppl. Fig 3A-D	Two-way ANOVAs P-Myrf(+/-), n=25 P-Myrf(-/-), n=25	**ROI**	**Effect**	**F**	**p**	**p (adjusted)**
		MTRHipp	MYRFGenotype	6.142	0.018	0.072
		MTRM1	MYRFGenotype	7.814	0.008	0.032
		MTRM2	MYRFGenotype	4.816	0.035	0.14

	Between subject factor: MYRFGenotype (2 Levels), Batch (4 Levels)	MTRS1	MYRFGenotype	13.376	<0.001	0.0032
Suppl. Fig. 3E	White matter skeleton - MTR Two-way ANOVA P-Myrf(+/-), n=25 P-Myrf(-/-), n=25 Between subject factor: MYRFGenotype (2 Levels), Wheel (2 Levels), Batch (4 Levels)	**Effect**	**DFn**	**DFd**	**F**	**p**
		MYRFGenotype	1	34	6.574	0.015
		Wheel	1	34	0.1	0.754
		Batch	3	34	4.91	0.006
		MYRFGenotype:Wheel	1	34	0.621	0.436

.055